AD-769 492

AN EXPERIMENTAL INVESTIGATION OF A HIGH LIFT DEVICE ON THE OWL WING

George William Anderson

Air Force Institute of Technology
Wright-Patterson Air Force Base, Ohio

March 1973

Unclassified
Security Classification

AD 769492

DOCUMENT CONTROL DATA - R & D

(Security classification of title, body of abstract and indexing annotation must be entered when the overall report is classified)

1. ORIGINATING ACTIVITY (Corporate author) Air Force Institute of Technology Wright-Patterson AFB, Ohio - 45433	2a. REPORT SECURITY CLASSIFICATION Unclassified 2b. GROUP

3. REPORT TITLE

AN EXPERIMENTAL INVESTIGATION OF A HIGH LIFT DEVICE ON THE OWL WING

4. DESCRIPTIVE NOTES (Type of report and inclusive dates)

AFIT Thesis

5. AUTHOR(S) (First name, middle initial, last name)

George W. Anderson
Captain, USAF

6. REPORT DATE	7a. TOTAL NO. OF PAGES	7b. NO. OF REFS
March 1973	86	21

8a. CONTRACT OR GRANT NO. b. PROJECT NO. c. N/A d.	9a. ORIGINATOR'S REPORT NUMBER(S) GAM/AE/73-6 9b. OTHER REPORT NO(S) (Any other numbers that may be assigned this report)

10. DISTRIBUTION STATEMENT

Approved for public release, distribution unlimited.

Approval for public release; IAW AFR 190-17 JERRY C. HIX, Captain, USAF Director of Information	12. SPONSORING MILITARY ACTIVITY Aeronautical Systems Division Wright-Patterson AFB, Ohio

13. ABSTRACT

A study was made of the aerodynamic function of the comblike fixtures found on the leading edge of owl wings. Microphotographs of an owl's wing showed the comb to resemble a row of spanwise twisted airfoils oriented to form a cascade. Smoke flow visualization tests on an owl wing showed that the comb acts as a cascade which turns the flow close to the wing leading edge in a spanwise direction. Flow visualization experiments were run using flat plate and cambered airfoils with combs in a low speed three-dimensional wind tunnel. Results showed that the leading edge comb produced a stationary spanwise vortex that delays flow separation at high angles of attack. The high lift device was related to the vortex lift phenomena observed on delta wing aircraft. The comb's small relative size, simple structure, and lack of moving parts may make it attractive for aircraft use.

DD FORM 1 NOV 65 1473

Unclassified
Security Classification

KEY WORDS	LINK A		LINK B		LINK C	
	ROLE	WT	ROLE	WT	ROLE	WT
Owl Wing						
Non-Linear Lift						
Cascade						
Bird Flight						
Vortex Sheet						
Leading Edge Separation						
Spanwise Flow						
Smoke Tunnel						
Flow Visualization						

AS NOTED IN THE NTIS ANNOUNCEMENT, PORTIONS OF THIS REPORT ARE NOT LEGIBLE. HOWEVER, IT IS THE BEST REPRODUCTION AVAILABLE FROM THE COPY FURNISHED NTIS BY THE CONTRIBUTOR.

AN EXPERIMENTAL INVESTIGATION OF

A HIGH LIFT DEVICE ON THE OWL WING

Thesis

GAM/AE/73-6

GEORGE W. ANDERSON
Captain USAF

ic

AN EXPERIMENTAL INVESTIGATION OF A HIGH LIFT DEVICE ON THE OWL WING

THESIS

Presented to the Faculty of the School of Engineering
of the Air Force Institute of Technology
Air University
in Partial Fulfillment of the
Requirements for the Degree of
Master of Science

by

George W. Anderson, B.S.
Captain USAF

Graduate Aerospace-Mechanical Engineering

March 1973

id

Preface

Bionics, the study of natural engineering systems, does not have a large representation in the literature of engineering. In fact, it is regarded by many as an unconventional approach to solving engineering problems. Such a stand disregards the wonderful advantage of having a working system or, in essence, the answer to the problem available for observation and experiment. With the answer already known, one can concentrate on understanding and to some degree duplicating the system.

I credit my introduction to bionics to Captain James Richmond recently graduated from the Aerospace Test Pilot School at Edwards AFB, California. His knowledge of the phenomena related to owl flight was the beginning of this study. The focus of the study on the leading edge comb of the owl wing was inspired by the book, Structure-Form-Movement, by Heinrich Hertel. In this book the function of the comb is identified as an unsolved problem in fluid dynamics. Most important, however, the study would not have been practical without the findings made by Dr. R.A. Kroeger of the University of Tennessee Space Institute in a wind tunnel test of the owl wing.

I made many friends in the engineering and biological sciences during my study of the owl wing. It would be less than fitting to omit the names of these who spent the most time in giving advice, direction, and encouragement in the study. Aeronautical engineers Jerry Martin and James Snyder of the Preliminary Design Division, Directorate of Advanced Systems Design, ASD, sponsored the project and acted as advisors. Professor Harold C. Larsen, Lt Colonel Frederick F. Tolle, and Captain R.F.

Bestgen were the AFIT faculty advisors. Captain Roger Crawford and Mr. Howard White of the Flight Dynamics Laboratory contributed their personal effort, technical library, and wind tunnel facilities. Finally, Mr. Robert Woods, Division of Wildlife, State of Ohio, and Mr. Richard Patterson of the Outdoor Education Center, Antioch College, made available live owls and a thorough background of the owl's habits and flight behaviour. To these people I owe not only the success of this project but also an increased appreciation for the bionic approach to engineering studies.

George W. Anderson

Contents

List of Figures

List of Tables

List of Symbols

A	Wing aspect ratio, b^2/S
b	Wing span
c	Wing chord
c_ℓ	Section lift coefficient
C_L	Total lift coefficient
$C_{L_{max}}$	Maximum lift coefficient
C_μ	Momentum coefficient
C_1	Constant of proportionality for non-linear wing-tip lift
D	Drag
L	Lift
$\dot{m}$	Mass flow-slugs/sec
q	Dynamic pressure
Re	Reynolds number, $\frac{\rho V \ell}{\mu}$
S	Wing area
V_j	Jet velocity, spanwise blowing
V_∞	Freestream velocity
W	Weight
α	Angle of attack
ρ	Mass density of air

Abstract

A study was made of the aerodynamic function of the comblike fixtures found on the leading edge of owl wings. Microphotographs of an owl's wing showed the comb to resemble a row of spanwise twisted airfoils oriented to form a cascade. Smoke flow visualization tests on an owl wing showed that the comb acts as a cascade which turns the flow close to the wing leading edge in a spanwise direction. Flow visualization experiments were run using flat plate and cambered airfoils with combs in a low speed three-dimensional wind tunnel. Results showed that the leading edge comb produced a stationary spanwise vortex that delays flow separation at high angles of attack. The high lift device was related to the vortex lift phenomena observed on delta wing aircraft. The comb's small relative size, simple structure, and lack of moving parts may make it attractive for aircraft use.

I. Introduction

Purpose

Achievement of higher lift coefficients at extremely low airspeeds is a problem of great importance in current STOL/VTOL aircraft development. In spite of intensive research in this area many of the current and proposed high lift systems suffer from serious shortcomings. Among these are excessive mechanical complexity and high engine thrust penalties. In view of these problems an ideal high lift device could be envisioned as one having no moving parts, no direct use of engine thrust, and negligible effect on high speed performance. The high lift device found on the wings of most species of owls deserves the aerodynamicist's attention in that it appears to have all of these ideal qualities. A previous wind tunnel study of an actual owl wing has identified the high lift function of a comb-like cascade located on the leading edge. Because of the limited nature of the study, no detailed data was gathered on the flow mechanism or performance of the high lift device. The purpose of this study was to identify the flow mechanism present on the owl wing and to produce a suitable analog or model of the device from which performance data could be measured in the wind tunnel. Further, recommendations are made as to the suitability of this device for use on conventional airfoils.

Method

The general method of study followed guidelines appropriate for a bionics type of investigation. The first step required examining and photographing the wings of live owls, obtaining components of owl wings for precise sectioning and measurement, and gathering data on owl flight from biologists and naturalists. Concurrently, a literature search was made to gather available data on aerodynamic theory relevant to bird flight. Following the physical study of the owl wing, enough data was available to design and construct a model of the leading edge comb. This comb was tested on several simple airfoils using flow visualization techniques in a three-dimensional wind tunnel. Insight gained in the flow visualization study suggested changes in the comb model until a close duplication of the flow over the owl wing was attained. Several flow visualization techniques were tried including smoke, titanium dioxide slurry, and tufts. The smoke tests proved to be the most successful and were used almost exclusively in the latter stages of the study. Observations from the smoke visualization showed the flow field to have many of the characteristics associated with the leading edge vortex phenomena observed on sharp leading edged delta wings operating at high angles of attack. The literature search was then directed toward studies in this area and was successful in locating material that aided in explaining the flow mechanism.

Background

The unusual configuration of the owl wing was first brought to the attention of the aeronautical engineering community in 1934 when Lieutenant Commander R.R. Graham, R.N. wrote an article on the subject in the Journal of the Royal Aeronautical Society (1). In this article entitled "The Silent Flight of Owls" Graham describes the hooked comb:

> "There is a remarkably stiff, comb-like fringe on the front margin of every feather that functions as a leading edge. The teeth of this comb are extensions of the barbs, or fibres, that form the front webb of the feather. They vary in length and distance apart

> according to the size o he bird and to their position in the wing. The large: of them are 4.0 mm. in length, and 0.75 mm. apart (1)."

This comb along with the other peculiarities of the owl wing was considered by Graham as contributing to the owl's quite flight. In the case of the comb, he proposes that aerodynamic quieting is caused by a reduction in flow velocity at the leading edge of the wing. Following Graham, a brief consideration of the comb's possible effect on sound generation is made by August Raspet in an article published in 1960 entitled "Biophysics of Bird Flight" (2). Raspet compares the combs to cylindrical wires generating aeolian tones and notes that the frequency of the emitted tone is a function of the cylinder diameter. In later years the common use of various types of vortex generators to delay flow separation on airfoils has promoted the theory that combs function in this manner and are not primarily intended for aerodynamic quieting. E.F. Blick of the University of Oklahoma states in an article entitled "Bird Ae-odynamics" that straight pins placed on the leading edge of an airfoil in an arrangement resembling the hooked comb results in an increase in lift (3). A recent NASA Technical Memorandum also shows that leading edge serrations result in significant increases in maximum lift coefficient by generating chordwise oriented vortices (4). The best presentation of the problem in engineering terms, however, appears in the book Struc.ure-Form-Movement by Heinrich Hertel (5). Here, the analysis considers shape, size, orientation, and applicable Reynolds number of the comb-wing system. Hertel makes the important observation that the hooked comb does not resemble the vortex or turbulence generators used on conventional airfoils because of the orientation of the comb blades relative to the airfoil surface. The conclusion that Hertel reaches is that the function of the comb is an unsolved problem in fluid dynamics (5). In 1972 an extensive study on owl flight was made by R.A. Kroeger and others at the University of Tennessee Space Institute (6). The study, entitled Low Speed Aerodynamics for Ultra-Quiet Flight, was a broad effort whose purpose was to measure the noise generated by the owl in flight and to identify any mechanisms that contributed to noise suppression. An important part of the study centered on the hooked comb configuration and involved a wind tunnel test of an owl wing. The results of this test showed that the comb delayed flow separation on the outer half of the wing up to extremely high angles of attack. By probing the flow field with tufts, a mapping of the streamlines over the top of the wings was obtained. This led to the discovery that the comb was producing a vortex sheet at the wing's leading edge and directing spanwise flow toward the wingtip. The data on streamlines and the discovery of the high lift function of the combs provided the basis on which the present study was undertaken.

II. Owl Wing Configuration

The configuration of the owl wing exhibits features common to most birds. The skeletal structure consists of a linkage of bones that closely resembles the human arm. In Figure 1 the analogy can be followed starting with the shoulder joint, progressing down the upper arm, and terminating at the wrist joint. Outboard of the wrist joint are bones controllable by the bird that terminate in feathers oriented at right angles to the direction of flight. These feathers are termed the primary flight feathers. Taken as a group they form a movable outer portion of the wing that is often referred to collectively as the manus. The feathers of the manus can be moved independently or as a group by the muscles. Filling out the remaining planform of the wing are the secondary feathers. These are held in place by the flesh or pataglum surrounding the bones of the forearm. The pataglum in addition to securing the secondary feathers also forms the contour of the leading edge of the inner portion of the wing. Projecting forward from the top of the wrist area are a grouping of two to three short feathers that act as a controllable aerodynamic "thumb". This feather system is called the alula or bastard wing and is well developed on the owl. The physical shape of the wing is completed by the presence of covert feathers which do not contribute to the planform of the wing but give it additional contour or thickness. The covert feathers are attached to the pataglum both above and below the main flight feathers and concentrate,additional thickness on the wing in the region directly behind the leading edge.

The primary and secondary feathers form the wing planform and are of special interest since they are also the wing's load carrying structure.

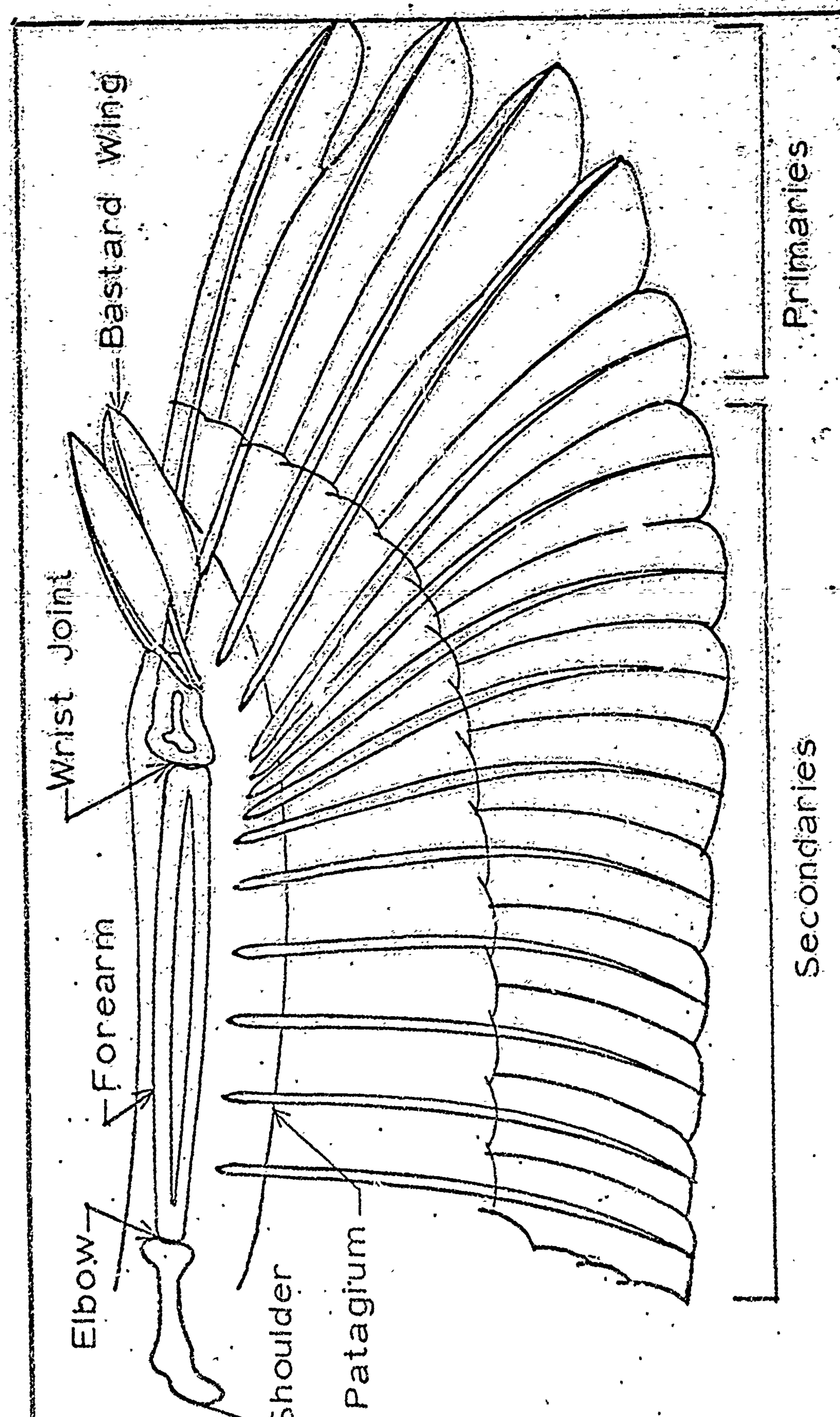

Figure 1. Owl Wing Configuration

These feathers are composed of a central shaft with vanes or surfaces running along most of its length. The vane is built up of a series of parallel rods or barbs that are bound together along their length by barbules. The barbules function in a manner analogous to hook and eye fasteners or, more closely, to the Velcro tape used as a fastener in some clothing. This feature allows the barbs to form a self-restoring surface when parted by abnormal local stresses.

It is obvious that the owl wing is a variable geometry device which integrates the bird's thrust and lift producing mechanisms as well as providing most of the means for flight control. These factors require the wing to change its shape and configuration and to change from an active to a passive role as thrust requirements dictate. One category of wing changes not under direct muscular control of the bird is the aeroelastic properties of the flight feathers. Aerodynamic forces acting on these feathers can be resolved into torsional and bending moments acting on the shaft. In-flight bending moments acting on the primary feathers of the manus cause the wingtip region to bend upward and open into a series of multiple airfoils. The orientation of these individual airfoils is not in the plane of the wing and varies with the owl's flight condition. A close examination of the manus region in Figure 2 shows that the first two primary feathers have their vane planform specifically designed to accentuate the slot effect. Bending effects on the secondary feathers result in a change in the physical camber of the inboard sections of the wing. Torsional moments about the feather shafts appear to play an important part in controlling the porosity of the wing surface. This porosity is formed by the slots that open between the flight feathers during the flapping or powered phases of flight. The

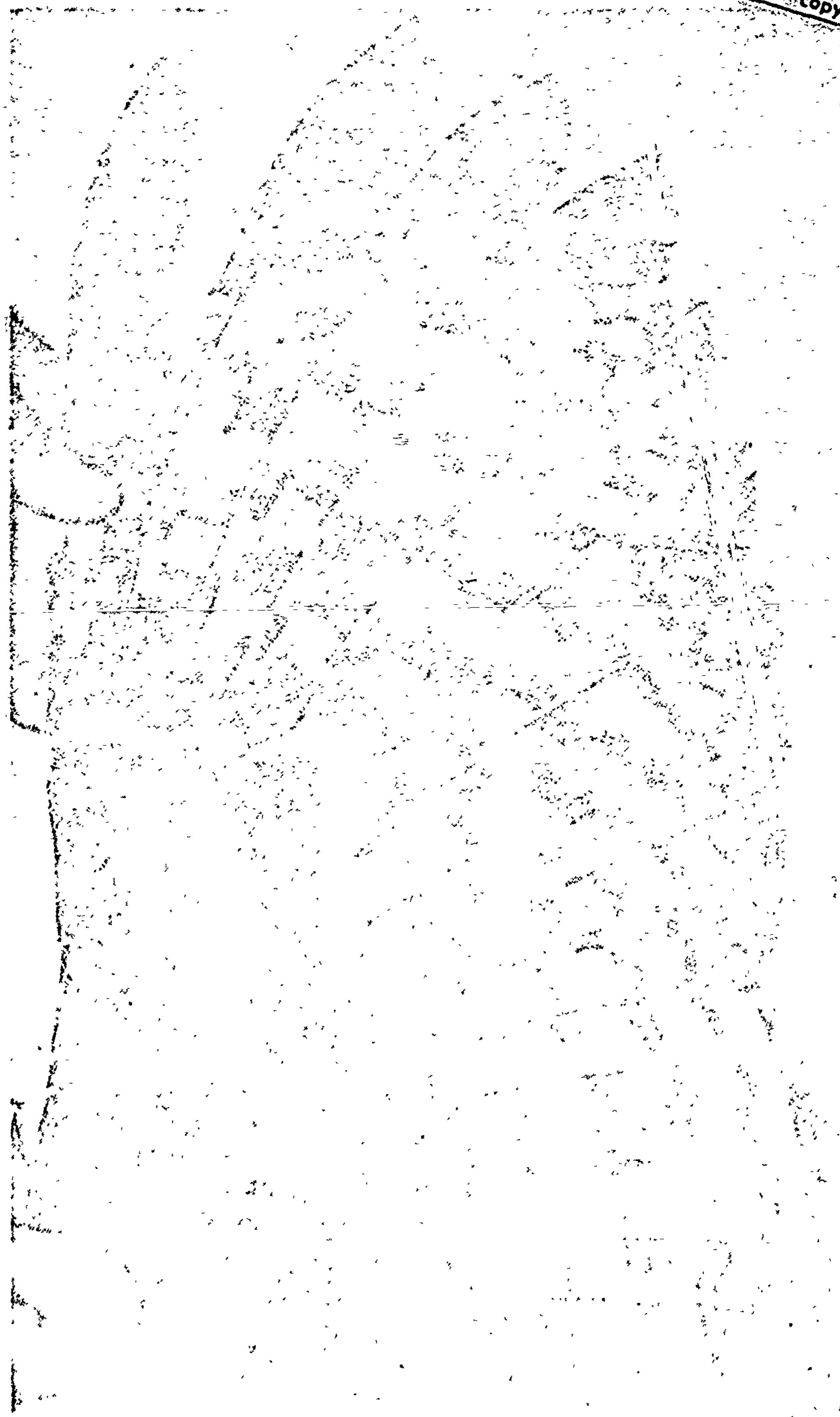

Figure 2. Planform of Great Horned Owl Wing

function and degree of this porosity is not well understood, however, several studies have been conducted in this field by the Russians (7,8).

The owl wing possesses a number of characteristics not generally found on other bird wings. The first of these is the hooked comb on the leading edge of the first and second primary feathers. Figures 3 and 4 show the comb position on the first primary feather. The comb is formed by the ends of the barbs that radiate from the shaft of the feathers. Toward the extremity of the barbs, the barbules that normally hold the vane together, part and allow the tip of the barbs to twist along their axis. It can be seen that the barbs taper sharply at the ends and retain the barbules on the outboard side. The size of the individual blades of the comb that is formed varies with the size and species of owl as well as with the position along the shaft of the feather. Representative dimensions are 2 mm. for the separated portion of the barb and 0.7 mm. between barb tips (5). A second peculiarity of the owl wing is the fringing that occurs in the vanes that make up the trailing edge portions of the wing. This is shown in Figure 5. Instead of binding the vane together out to the apex of the barbs, the barbules again release their hold and the resulting separation of the barbs forms a discontinuous surface. The appearance of the separated barbs is quite different from that of the leading edge comb. On the trailing edge the barbs form soft, flexible streamers from which minute barbule filaments radiate in all directions. The final characteristic is the downy upper surface on the portions of the vanes that come in contact with adjacent feathers during flight. The contrast between downy and smooth areas on the upper vane surfaces is shown in Figures 6 and 7. Because the downy surfaces are present only in areas of physical contact, it is presumed

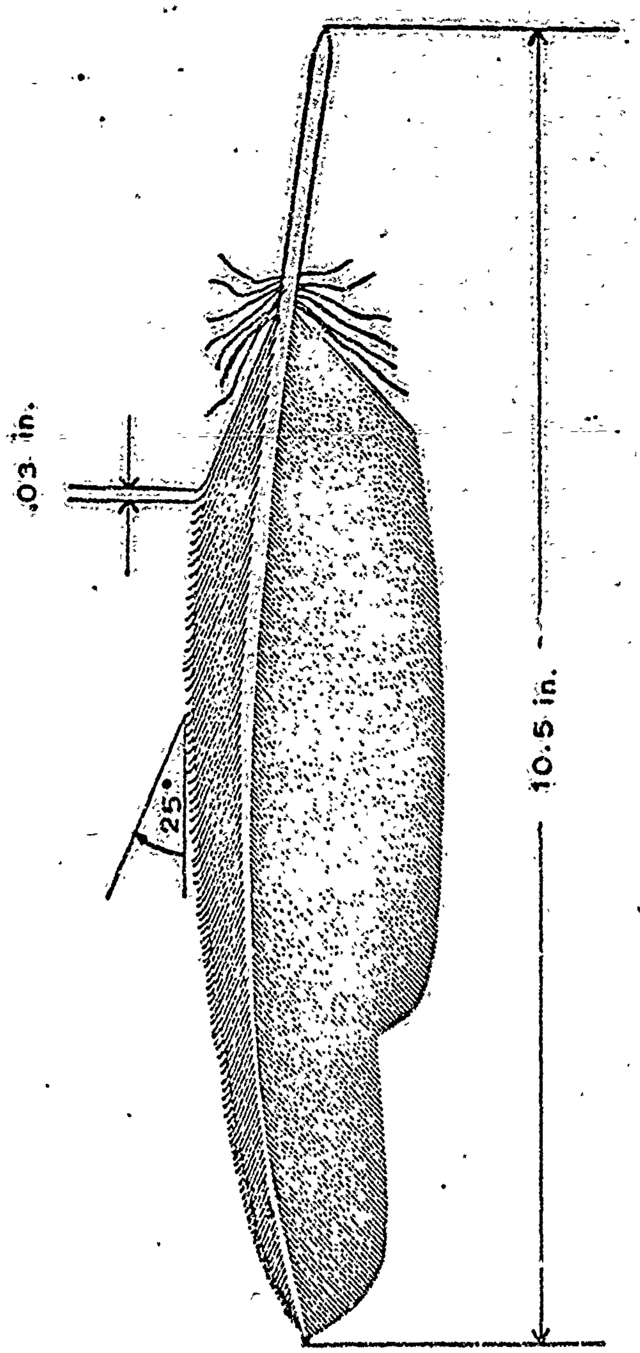

Figure 3. First Primary Feather with Hooked Comb

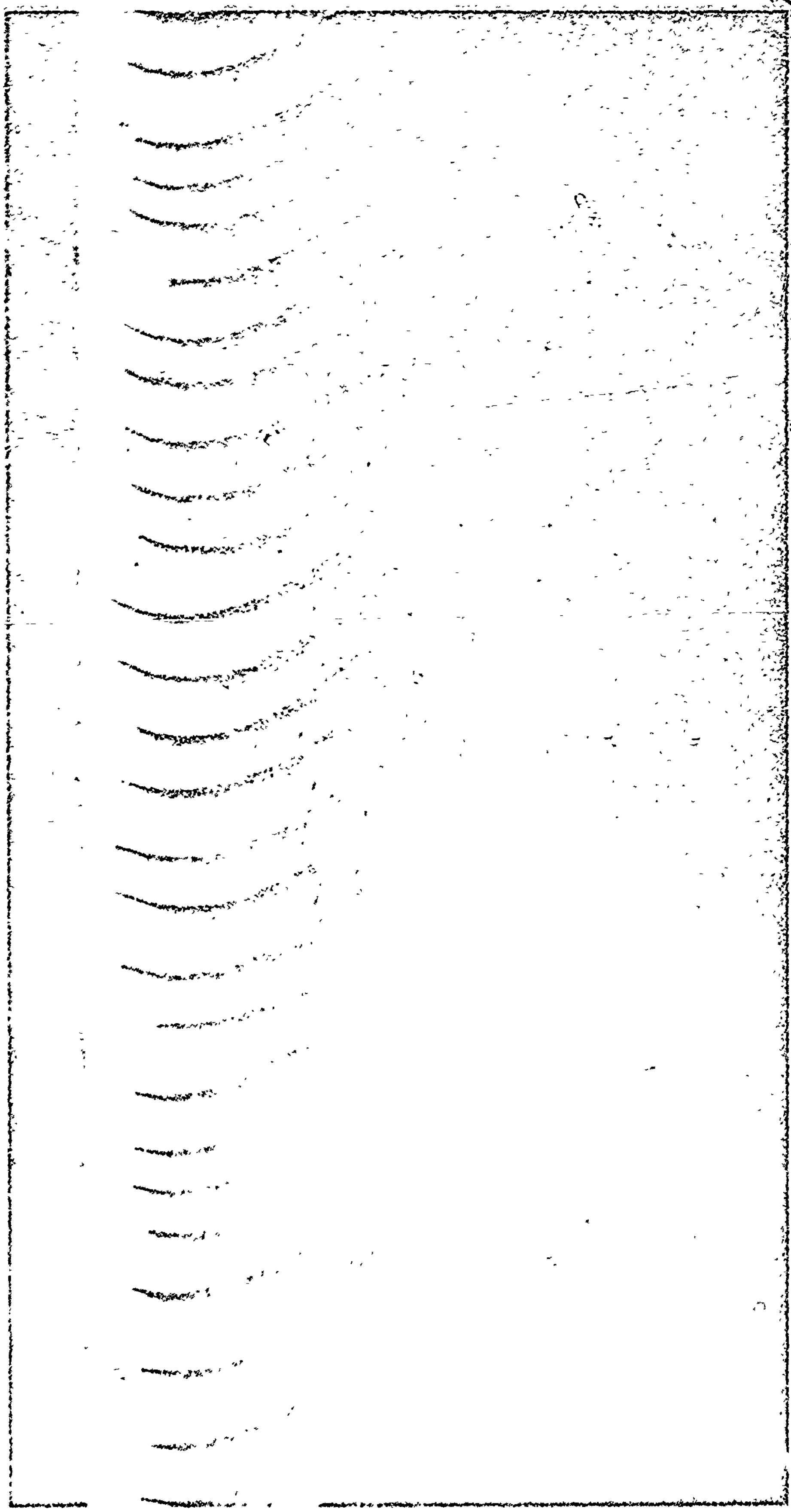

Figure 4. Hooked Comb Magnified 20X
(The Wingtip is to the left)

that they perform either a lubricating or quieting function (5).

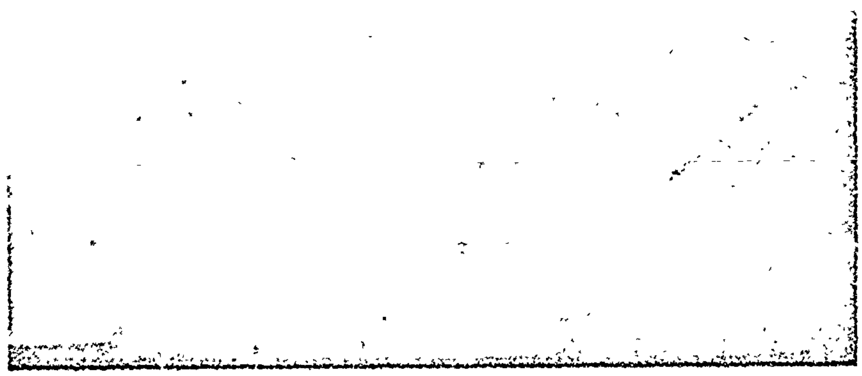

Figure 5. Trailing Edge Fringing Magnified 30X

Figure 6. Smooth Feather Vane Surface

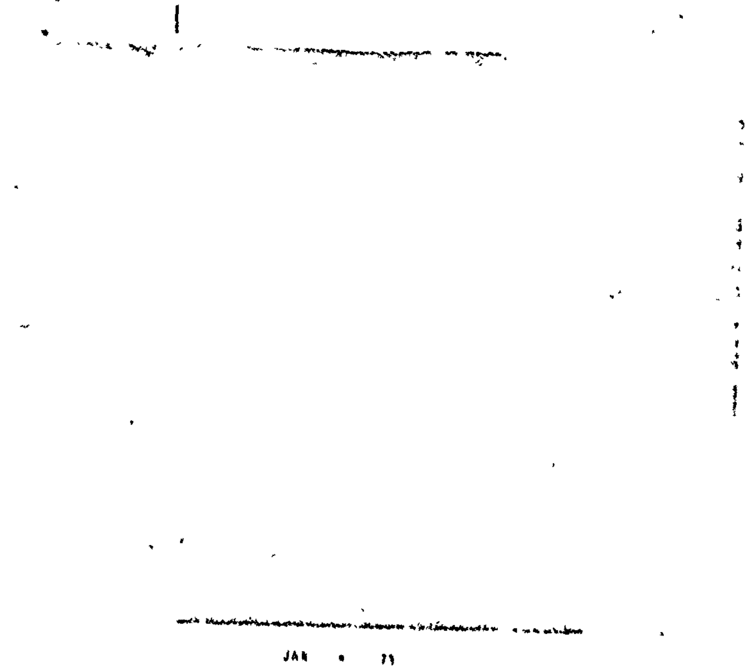

Figure 7. Downy Feather Vane Surface

III. Literature Survey of Test Data

The study of owl flight by Kroeger (6) contains a great deal of data on the aerodynamic performance of the individual devices present on the owl wing. The data relevant to the hooked comb problem falls in three main categories. These are wind tunnel tests of a severed owl wing, water tunnel tests of a hooked comb analog, and free flight experiments using live owls. Each of these experiments is discussed with respect to their contributions to the understanding of the function of the hooked comb.

Wind Tunnel Test of Owl Wing

A small owl wing was placed in a low speed wind tunnel and the flow over the wing studied with smoke visualization and tufts. Kroeger found that the smoke flow over the outer half of the wing varied with angle of attack. As shown in Figures 8 and 9, the flow over the wing turned inboard at low angles of attack and outboard at high angles of attack. An examination of the flow pattern on the upper wing surface also revealed marked variations with angle of attack. At low angles of attack, the streamlines were primarily chordwise and no effect of the leading edge comb on the flow field could be seen. At high angles of attack, the comb created a spanwise flow toward the wingtip. This spanwise flow is shown in the surface streamline sketch of Figure 10. In addition to creating this spanwise flow component, the combs generated a vortex sheet at the wing leading edge. This vortex sheet extended from the bastard wing at mid-span out to the tip of the first primary feather. The action of the vortex sheet appeared to delay flow separation on the outer half of the wing to an angle of attack in excess of

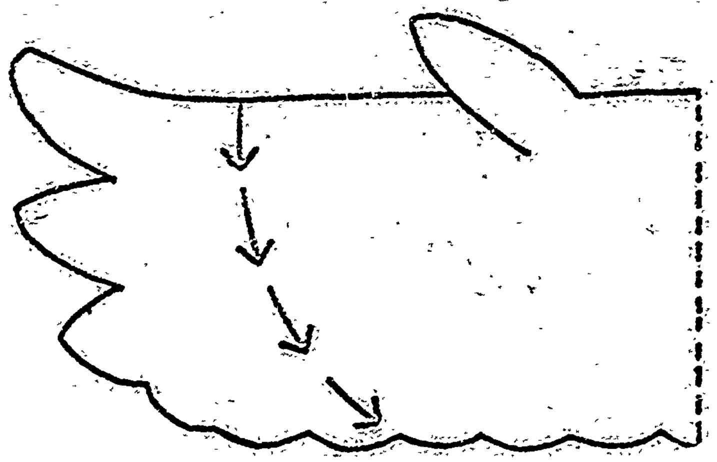

Figure 8. Flow Over the Owl Wing at Low Angles of Attack

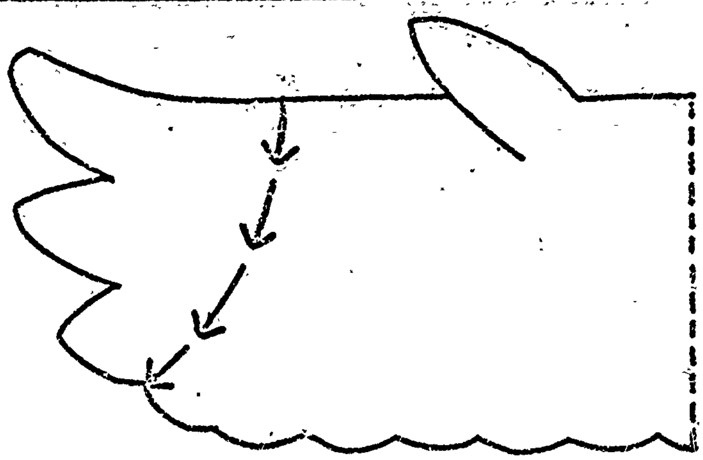

Figure 9. Flow Over the Owl Wing at High Angles of Attack

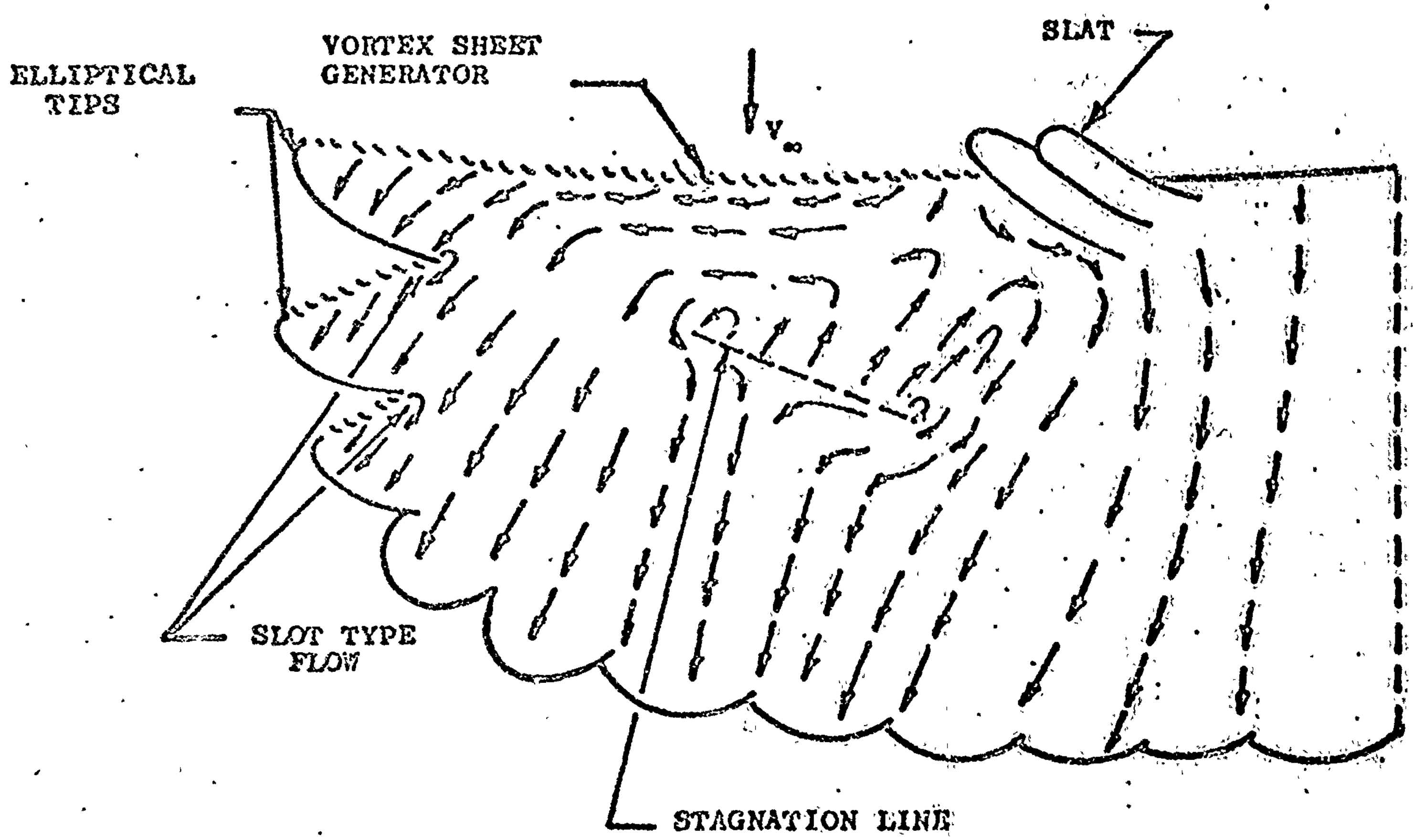

Figure 10. Streamlines on Upper Wing Surface at High Angle of Attack (6)

30 degrees. When the comb was removed from the leading edge, the wing stalled at a much lower angle of attack and a mapping of the surface flow (Figure 11) indicated that the spanwise vortex sheet was absent. Kroeger reported that the comb's effect on the flow field was highly three dimensional. As shown in Figure 12, the turning of the flow through the comb is highest at the wing surface and decreases with increasing distance from the wing surface until the flow is chordwise at the comb tips. No deformation of the comb occurred during these tests in spite of the small relative size of the individual teeth. In explaining the overall flow field on the upper wing surface, Kroeger suggests that the vortex sheet and the unusual counterrotating flow fields at mid-chord are created by the mutual action of the hooked comb, the bastard wing, and the slotted wingtip.

Water Tunnel Experiment

Kroeger attempted to duplicate the vortex sheet flow created by the comb system in a small water tunnel. The shape shown in Figure 13 proved successful. The comb was made of .0014 shim stock and each of the blades were twisted until the tips had a zero angle of attack with respect to the free stream. Although the analog appeared to create a vortex sheet downstream of the comb, no tests were conducted to measure its function as a high lift device.

Free Flight Test of Live Owls

A Barred owl (Strix varia alleni) was used in Kroeger's flight tests. The owl was constrained to fly a relatively fixed flight path and measurements were taken by means of photographs. By computing velocity and glide angle during the gliding portions of the owl's flight,

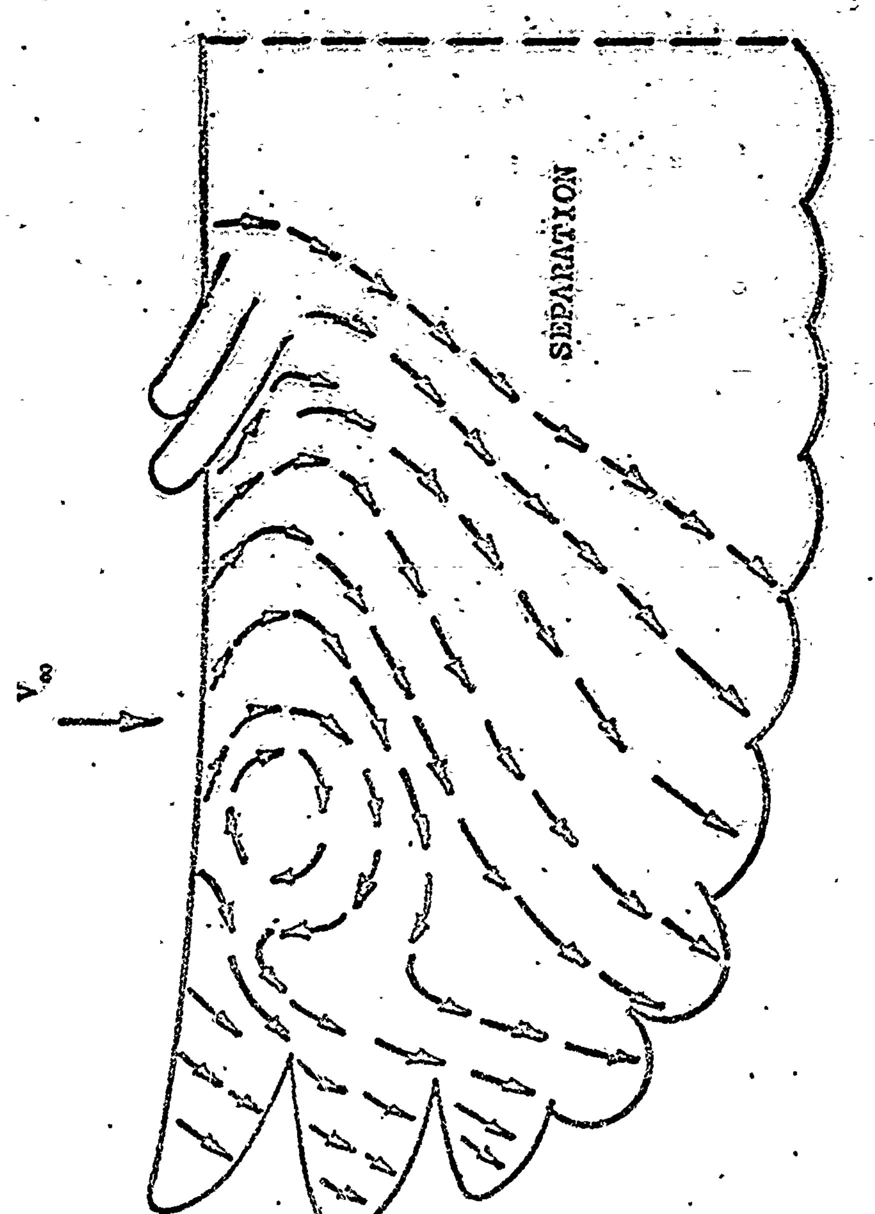

Figure 11. Streamlines on Upper Wing Surface at High Angle of Attack and Leading Edge Comb Removed (6)

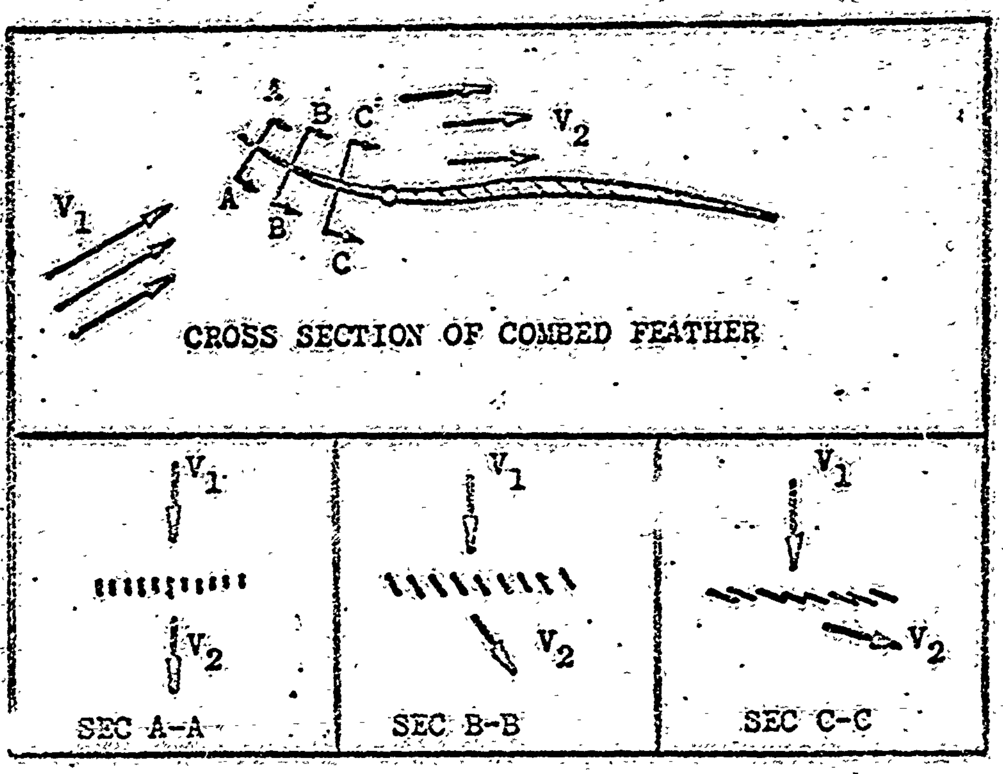

Figure 12. Flow Turning Created by the Hooked Comb (6)

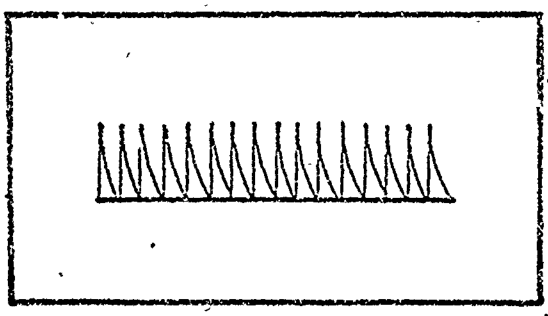

Figure 13. Comb Shape Used in Water Tunnel Experiment (6)

average Reynolds number and L/D values were obtained. At a Reynolds number of approximately 1.3×10^5, Kroeger reports the owl's gliding L/D to be on the order of two. This is very low performance when compared to reported values of 16 to 20 for a soaring black buzzard (6). Later modifications of the owl's wing including removal of the leading edge comb failed to produce any noticable change in flight performance. This result tended to indicate that the full aerodynamic capability of the wing was not used at the high glide angle used in the experiment.

IV. Physical Characteristics of Owl Wings

General Features

Owls are classified in the biological order strigiformes. Most of the members of this order have the hooked comb configuration. For this investigation two species of live owls were studied, the great horned owl (bubo virginianus) and the barn owl (tyto alba). The planforms of their wings are shown in Figures 14 and 15. In both photographs the hooked comb is plainly visible on the first primary feather. The wing of the great horned owl is held in a position close to that observed in gliding flight. The outline of the wing shows it to have an untapered inboard section with an elliptically shaped tip or manus region. Also, the individual primary feathers exhibit elliptical tips. The bastard wing is located at the approximate mid-point of the leading edge and is faired into the surrounding covert or contour feathers. The covert feathers, especially on the inner wing, are extremely light and downy. This characteristic lends credence to the theory held by several authors that the coverts form a compliant surface that functions to delay boundary layer transition (5,9). This ability of a compliant surface to delay transition has been established by Kramer (10). Several flights of the great horned owl were observed. The owl was induced to fly between elevated perches in an outdoor enclosure 40 feet long. On most of the flights the owl flew directly over the observer at heights of 2-3 feet. A number of characteristics were noted during the flights:

1. The owl has an extremely long glide phase during which the wing remains relatively fixed in planform

Figure 14. Wing Planform of Live Great Horned Owl Bastard Wing Located Forward at Mid-Span

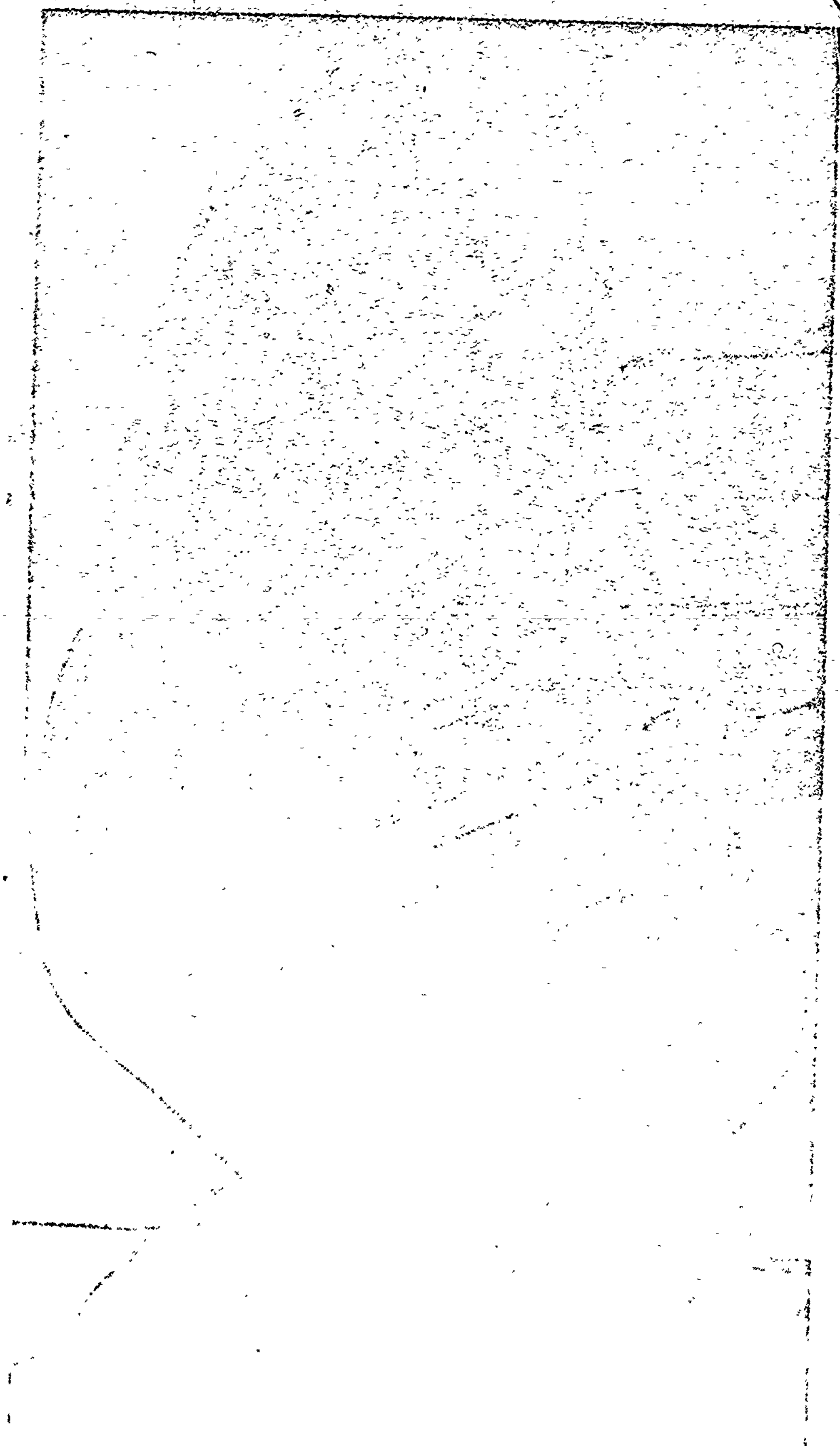

Figure 15. Wing of Live Barn Owl

and sweep. Figure 14 shows the wing held in a position close to that observed in flight.

2. The bastard wing was held slightly open and swept forward.
3. The deflection of the primary feathers was small but the tip slots were clearly visible.
4. The glide angle was approximately 15 degrees.
5. Openings were not visible between the secondary feathers during the gliding phase.

Wing Measurements

Detailed measurements of an owl wing were made to study its aerodynamic characteristics. The wing was formed into a gliding configuration and the measurement in Table I taken. Since the weight of the owl was not available it was computed using the wing loading value typical of this species (11). The flight Reynolds number was based on the chord length taken at mid-span and a velocity of 25 ft/sec. The wing loading value of .637 lbf/ft^2 is close to that measured for other predator birds such as hawks but is very low compared to conventional aircraft. By comparison, the U-10D Helio Courier aircraft which is capable of excellent STOL performance has a wing loading of 14.7 lbf/ft^2 (12). Figures 18 and 19 show the wing sections that were taken at representative positions along the span. All the sections resemble conventional airfoils in that they can be described by distributing a thickness envelope over a camber line. Section 1 was taken in the region between the wing root and the wrist area. This represents the thickest part of the wing and is highly cambered. Section 2 taken between the wrist and the end of the region covered by covert feathers

Table I

Measurements of Severed Great Horned Owl Wing

Weight, lb*	1.7
Wing area**, in^2	398
Wing Span, in	48.0
Wing sweep angle, deg.	0
Chord at half span, in	10.
Wing loading, lb/ft^2	0.64
Wing aspect ratio	5.8

Table II

Owl Wing Section Measurements

Section	Chord (c), in	Camber	Camber Position	Max. Thickness	Leading Edge Radius
1	9.7	.14c	.32c	.08c	.03c
2	9.5	.09c	.44c	.07c	.03c
3	9.4	.08c	.41c	.03c	sharp
4	8.1	.09c	.51c	.02c	sharp

*Weight calculated from wing loading value of reference 5.
**Wing area includes the body area intercepted by the wing.

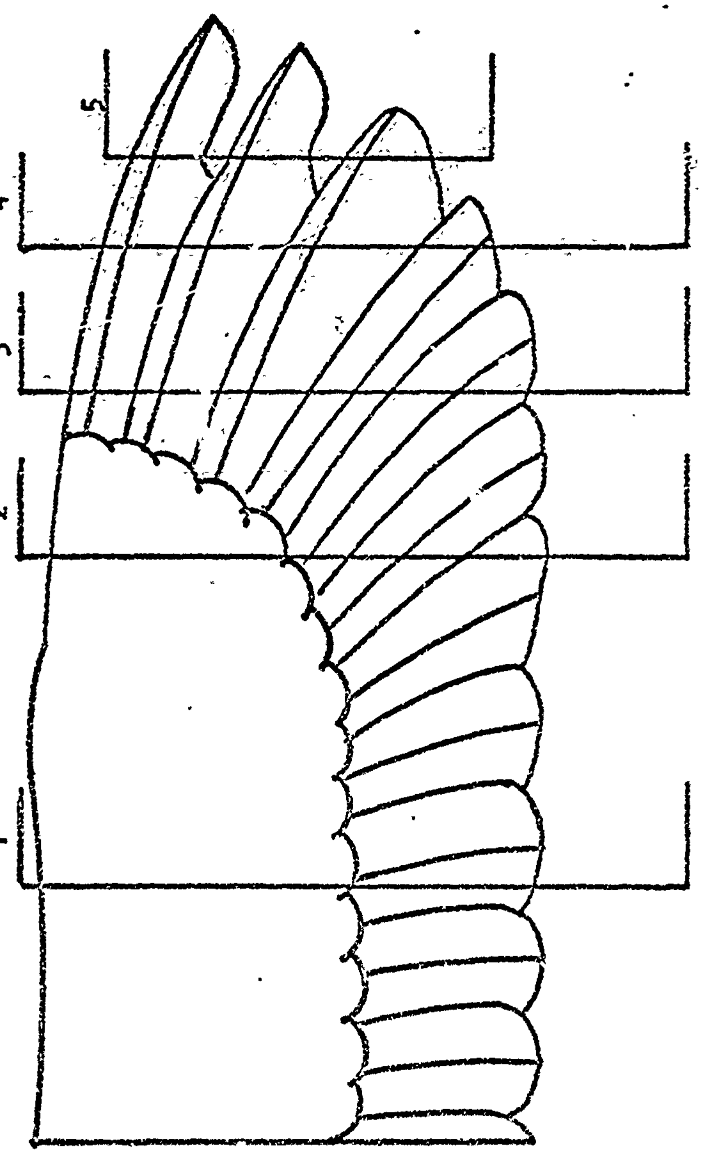

Figure 16. Owl Wing Sections

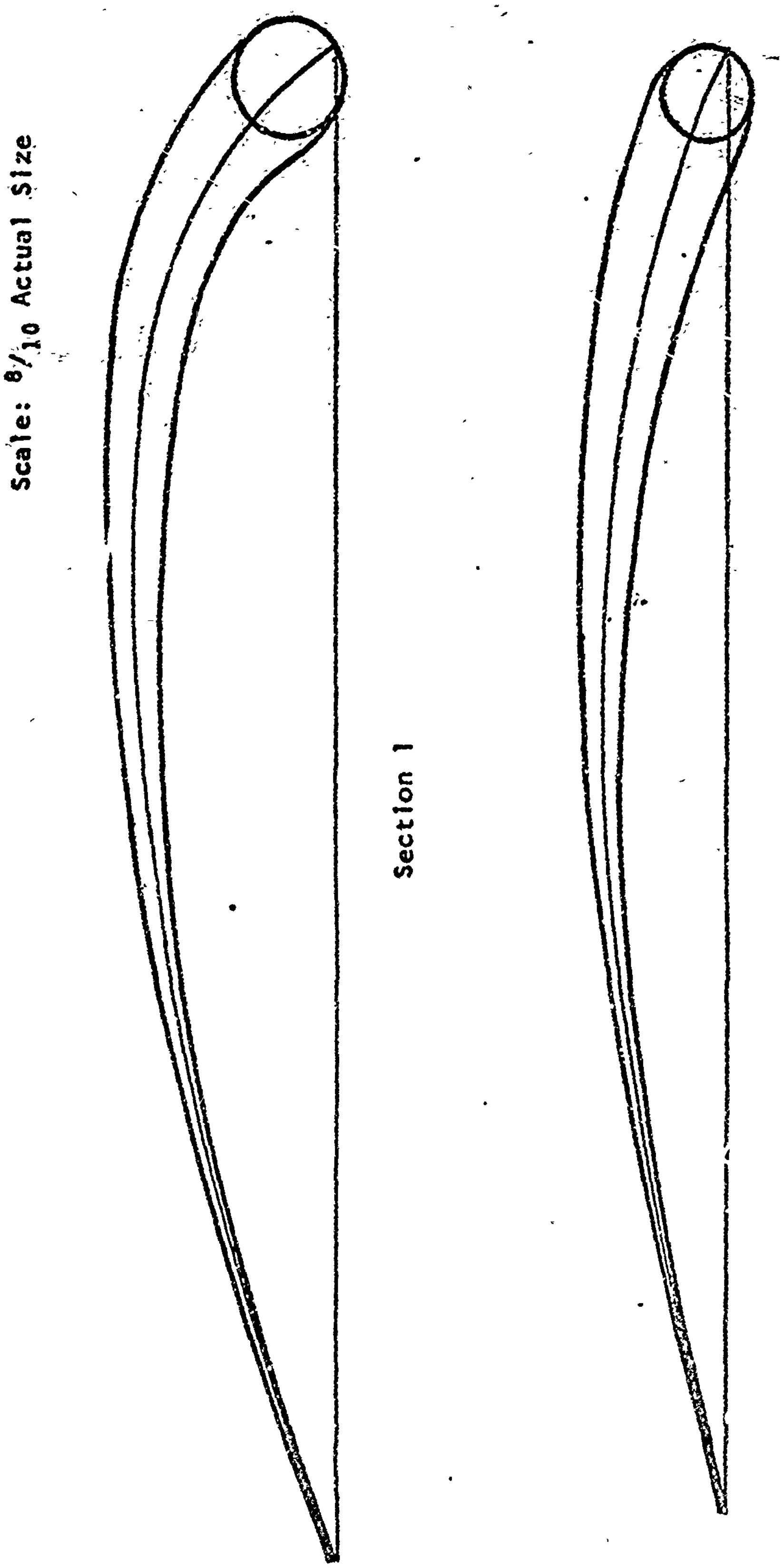

Figure 17. Wing Sections 1 and 2

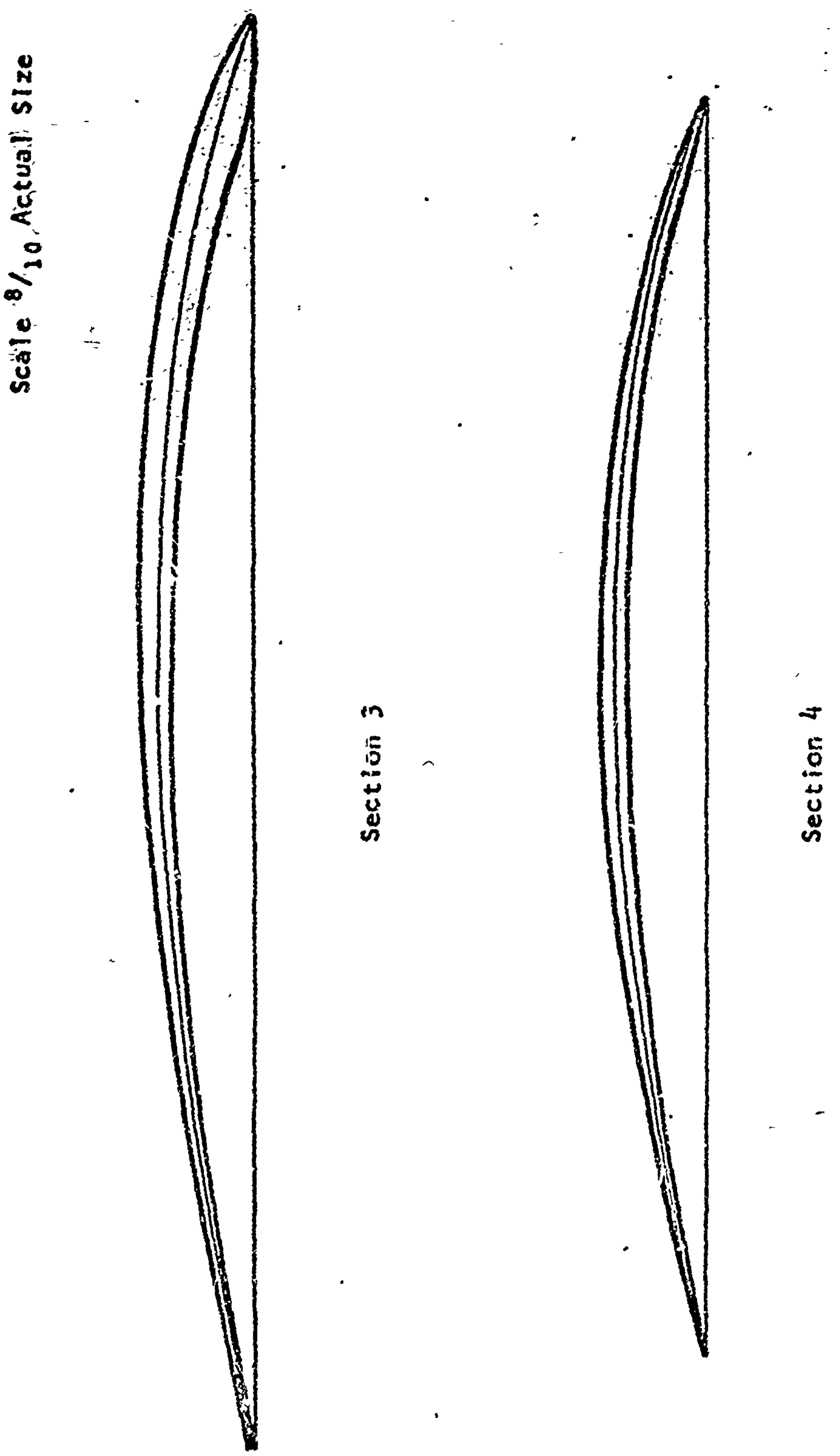

Figure 18. Wing Sections 3 and 4

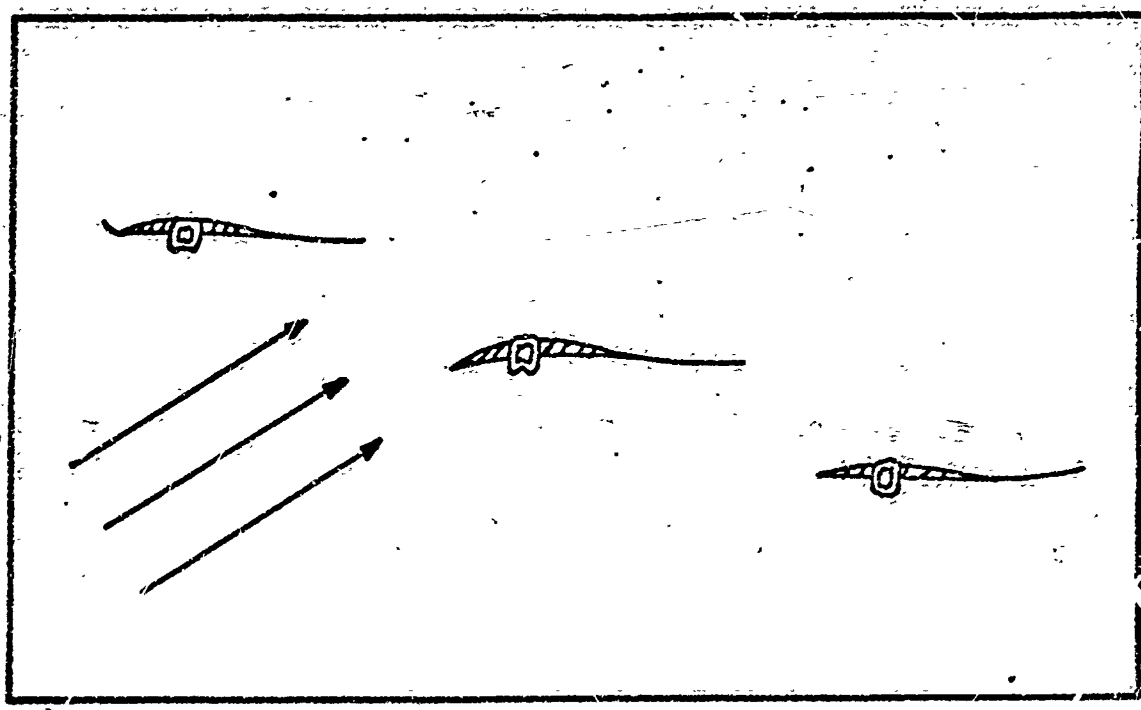

Figure 19

Section 5. Position of Tip Feathers Under Aero-elastic Deflection During Gliding Flight

remains fairly thick but has reduced camber. A marked change in shape occurs in sections 3 and 4. These sections are located in the manus region where the surface is composed of only the primary feathers. Both sections have sharp leading edges, low relative camber, and small thickness. Outboard of section 4 the wing breaks into a series of multiple airfoils. The relative positions of these airfoil sections are shown in Figure 19. Considering the structure of the wing, changes in the geometry of the inboard sections during gliding flight should be relatively small. Table II lists the section values of camber, maximum thickness, and leading edge radius. Using these values, the following comments can be made:

1. Section 1 has a maximum camber of 14% which is much higher than on conventional airfoils where values rarely exceed 4%. This high camber suggests high section $C_{l_{max}}$ and large pitching moments (13).
2. Sections 3 and 4 have thicknesses below the minimum value of 4% usually given as a structural limit in preliminary aircraft design (14).
3. The maximum thickness on section 4 is located behind mid chord suggesting a large percentage of laminar flow.

Hooked Comb

In order to model the hooked comb, its exact shape and orientation was studied. Since the comb is too small to inspect without magnification, a laboratory comparator was used to select sections for microphotography. A 35 mm single lens reflex camera with bellows attachments giving negative magnifications of 10-30X was found to be suitable. Microphotographs of the comb are presented in Figures 20 through 26. Figure 20 shows a top view of the comb system magnified 30X. Even at this high magnification, the surface formed by the barbules appears to be fairly solid except for the fringing at the tips. Separation of the barbules from the adjoining barb occurs some distance prior to the beginning of the taper in the outer portion of the comb. Because of this, the barbule surface overlaps the adjoining barb for a short distance. This characteristic cannot be fabricated in a model cut from a flat sheet. Figures 21 and 22 show the comb from the direction of the free stream when the wing is at an angle of attack of 30 degrees. In

Figure 21 a cascade is formed by the barbules which resemble a series of individual blades and turn the flow toward the wing tip. If the individual barbule surfaces are assumed to be relatively impermeable, the ability of the cascade to turn the flow may be quite high. A primary variable in cascade geometry is blade solidity, defined as the ratio between blade chord length and blade separation. In this cascade the solidity is quite high in the base region and tapers off toward the tip as the barbule chord length decreases.

Figure 22 shows the shape of the barbs on the underside of the wing surface. The shape remains rectangular until reaching the comb where it changes sharply and becomes cylindrical. A critical parameter in specifying the orientation of the barbs is the angle at which they radiate from the vane axis. This value is approximately 25 degrees and varies little along the span of the feather. This contrasts with the large variations in barb angle present on a flight feather without the hooked comb. Further insight into the shape of the individual blades or barbule surfaces can be gained by sectioning a single barb from a leading edge primary feather and photographing it from several angles. The photographs in Figures 23 through 26 show the barb in the top, left side, and two oblique views. (The hole appearing in all views was made by a pin during sectioning.) The top and side views show the twist of the barb along its axis. No twist could be seen in the barbule surface about the barb axis.

Conclusions

A number of conclusions were made after considering the owl's wing structure and aerodynamic performance:

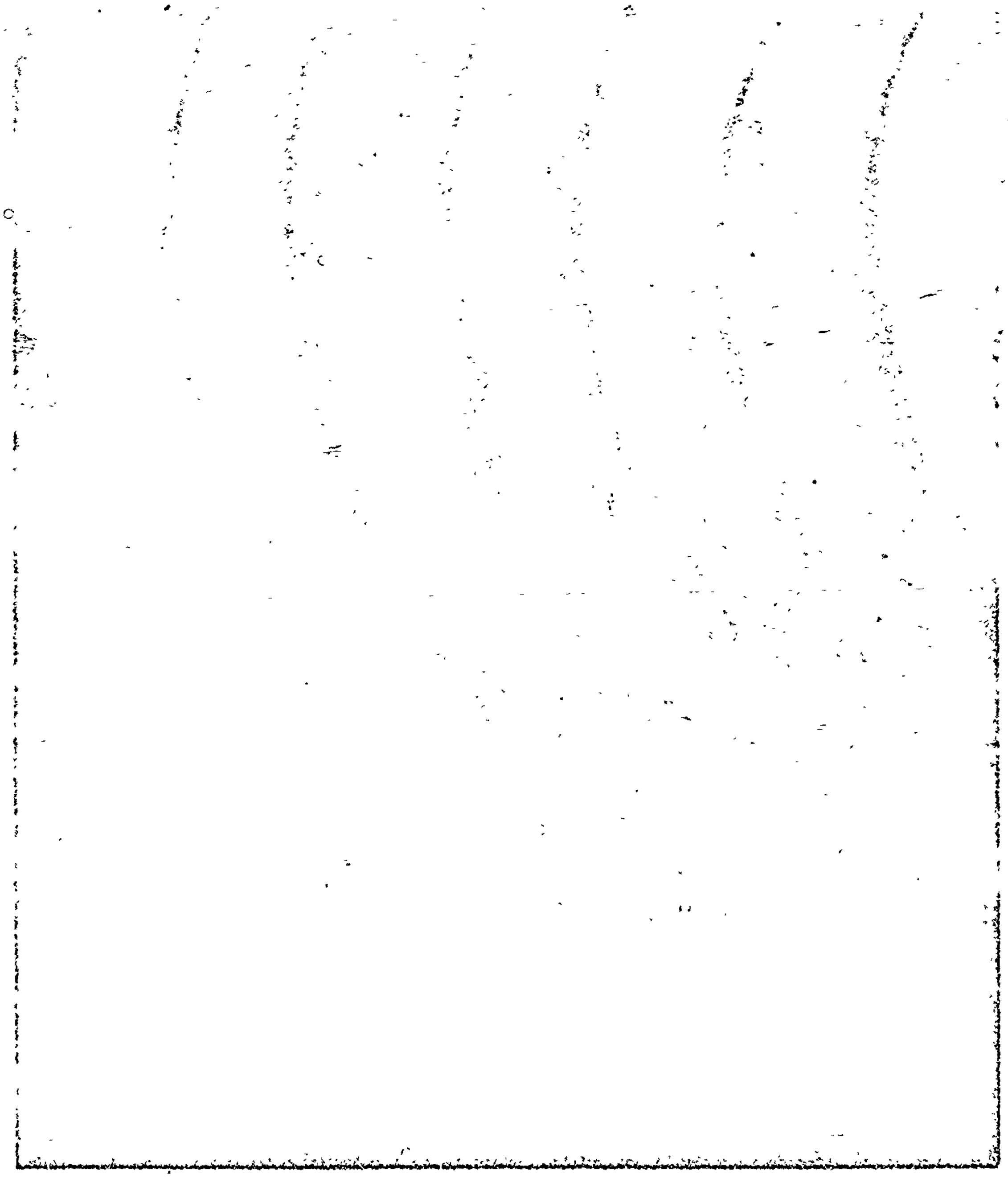

Figure 20. Comb Blades Magnified 30X

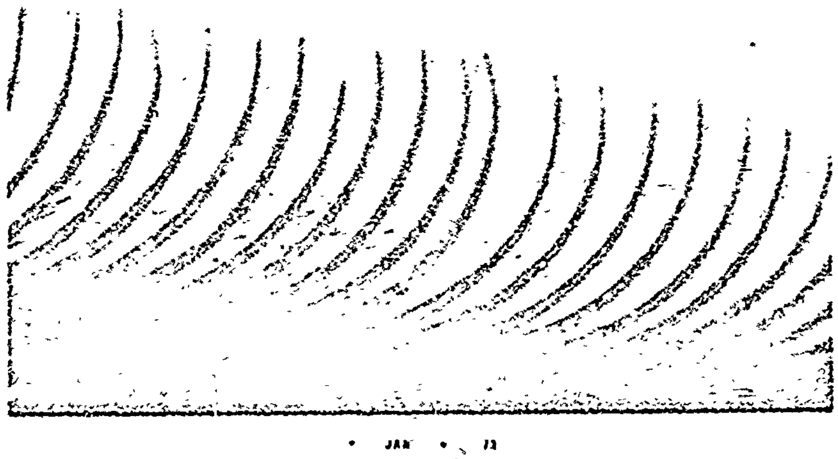

Figure 21. View of Comb from Free Stream Direction

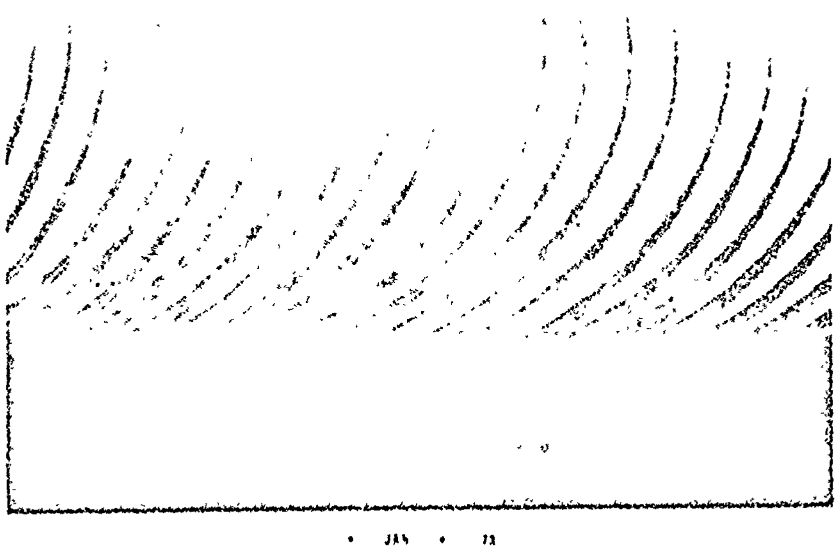

Figure 22. Barbule Structure in Base Region

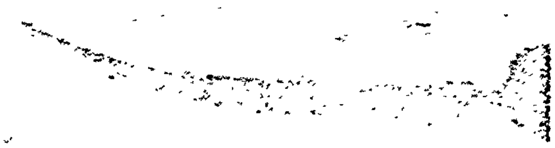

Figure 23. Comb Blade, Top View

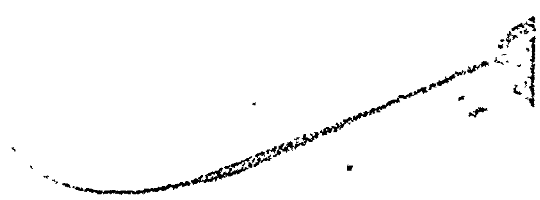

Figure 24. Comb Blade, Side View

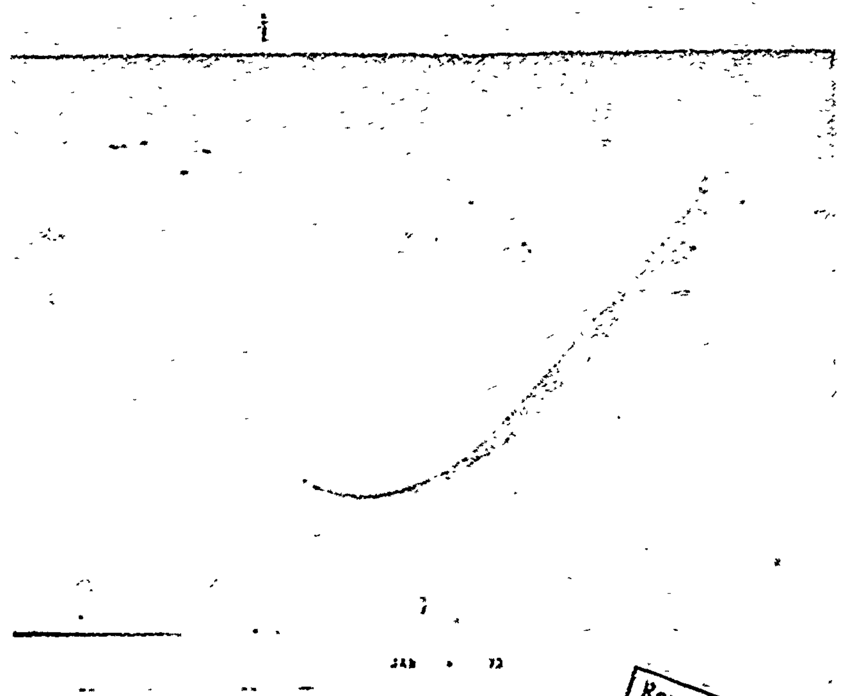

Figure 25. Comb Blade, Left Oblique

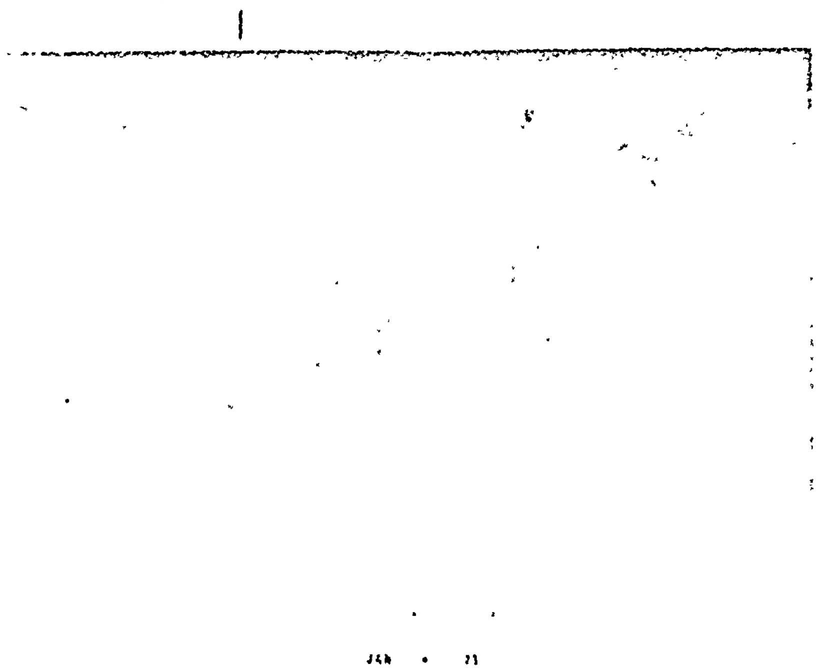

Figure 26. Comb Blade, Right Oblique

1. The great horned owl was capable of higher gliding values of (L/D) than reported by Kroeger. This may suggest why Kroeger's removal of the leading edge comb failed to cause a change in the owl's gliding performance.
2. The bastard wing is used during gliding flight.
3. Except for the tip region, the wing could be considered an unbroken surface during the gliding phase.
4. The wing sections in the region of the comb are thin and have sharp leading edges.
5. The hooked comb shape with the exception of the barbule overlap in the base region can be fabricated from a flat sheet.
6. An important parameter in constructing the comb appears to be the 25 degree angle at which the axis of the barb radiates from the feather vane.

V. Experimental Equipment and Model Description

Wind Tunnels

Two wind tunnels were used during the course of this study. Most of the work was done in the 3-foot tunnel belonging to the AF Flight Dynamics Laboratory. This tunnel is an open circuit, closed test section unit capable of velocities up to 30 ft/sec. The physical layout of the tunnel (Figure 27) consists of a wooden tube measuring 3 feet in diameter and ten feet long. The airflow is controlled by a variable speed DC motor installed at the exit of the tunnel. The motor drives a three-bladed propeller located behind adjustable guide vanes that reduce undesirable rotational velocities in the test section. Turbulence reduction is accomplished by use of a removable honeycomb section placed in the tunnel entrance. The test section is viewed through a large plexiglass window on the right wall of the tunnel and accessibility to models is afforded by a port on top. During this test the tunnel was equipped with a commercially manufactured smoke generator called the "Cloud Maker" (Testing Machines Inc.). This unit produces a thick white smoke by evaporating mineral oil. A high pressure bottle of carbon dioxide is used to force the smoke into a glass jar which acts as a reservoir. From the reservoir the smoke is injected into the tunnel through a rubber tube connected to a 3-foot section of 3/16" diameter stainless steel tubing. To obtain multiple smoke streams, a second tunnel was used briefly. The tunnel belonged to the AF Aerospace Research Laboratory (Figure 28). It consists of a closed section, open circuit unit with a 1' x 1' square test cross section. Air enters the tunnel through ten screens and is contracted in a nozzle before reaching

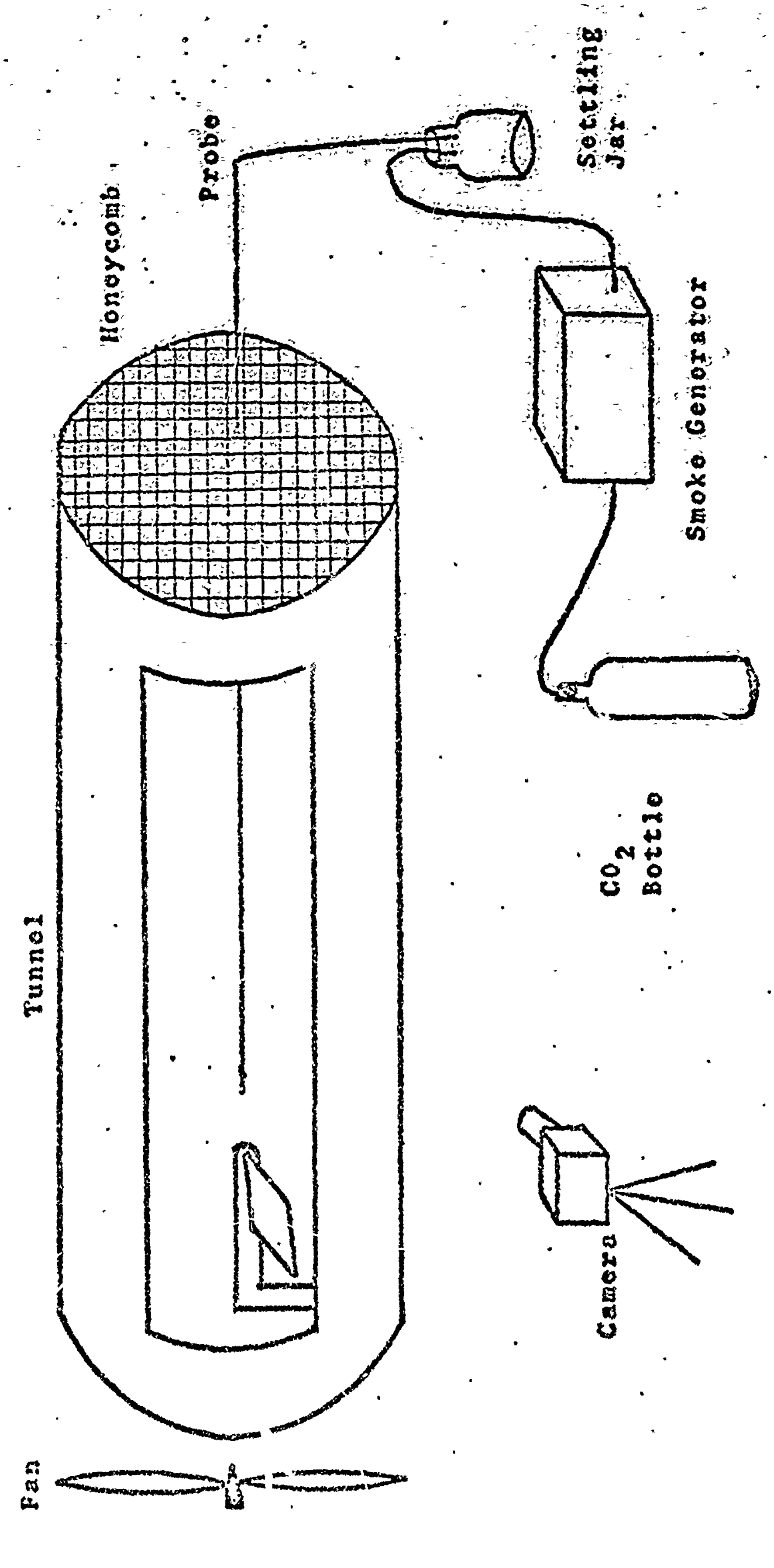

Figure 27. FDL Three Foot Wind Tunnel

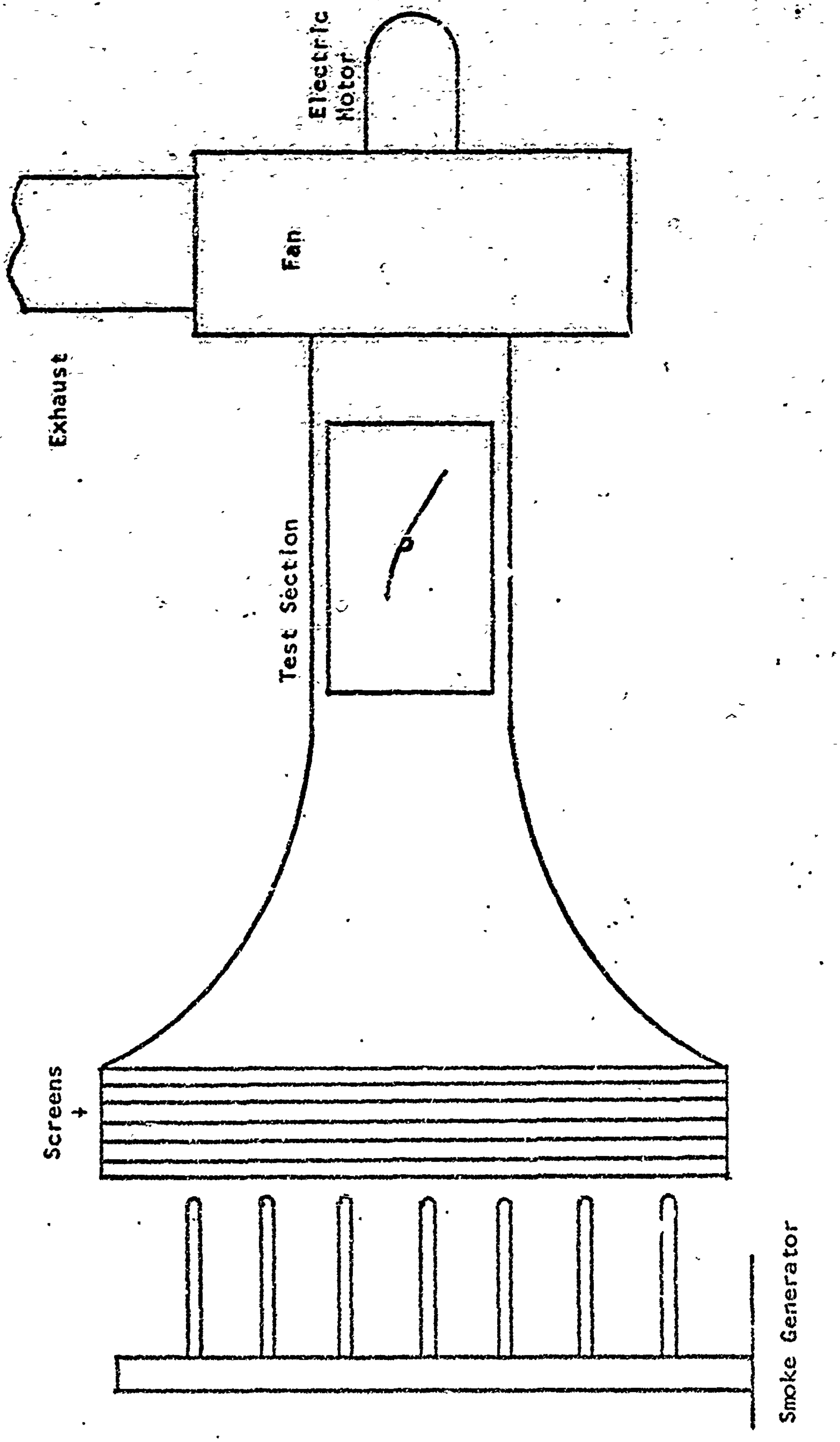

Figure 28. ARL Low Turbulence Wing Tunnel

the test section. Air flow is induced by a ½ hp constant speed motor. Velocity is controlled by adjusting louvers in the fan section. Smoke is generated by evaporating kerosene using an electric heating element. The smoke is injected into the tunnel through 7 pipes placed in front of the entrance screens. Because of the multiple screens and the high contraction ratio of the nozzle, extremely low turbulence flow is produced in the test section.

Photography

Pictures of the smoke flow patterns required a very high speed film. The film was Polaroid Type 57 with an ASA 3000 speed. The camera was a Graflex 4X5 used in conjunction with a high intensity stroboscopic light source. Best results were obtained with camera settings of f16 at 1/100 sec.

Models

Airfoils. Three airfoil shapes were used in the experiment. All were cut from .065" aluminum sheet and had sharpened leading edges. The planform and camber of the models are shown in Figure 29. Model A was a flat plate with an elliptically shaped tip. Model B was similar in planform but had circular arc camber. Model C was cambered only on the forward position of the wing and had a rectangular shaped tip. The models were supported in the tunnel by the sting system shown in Figure 27. To minimize interference effects of the mounting and provide an end plate for the wing root, a 10" x 10" aluminum plate could be attached to the sting at the wing root.

Hooked Comb. The best fabrication results were attained with .004" brass shim stock, which is easily cut with small scissors and can be shaped

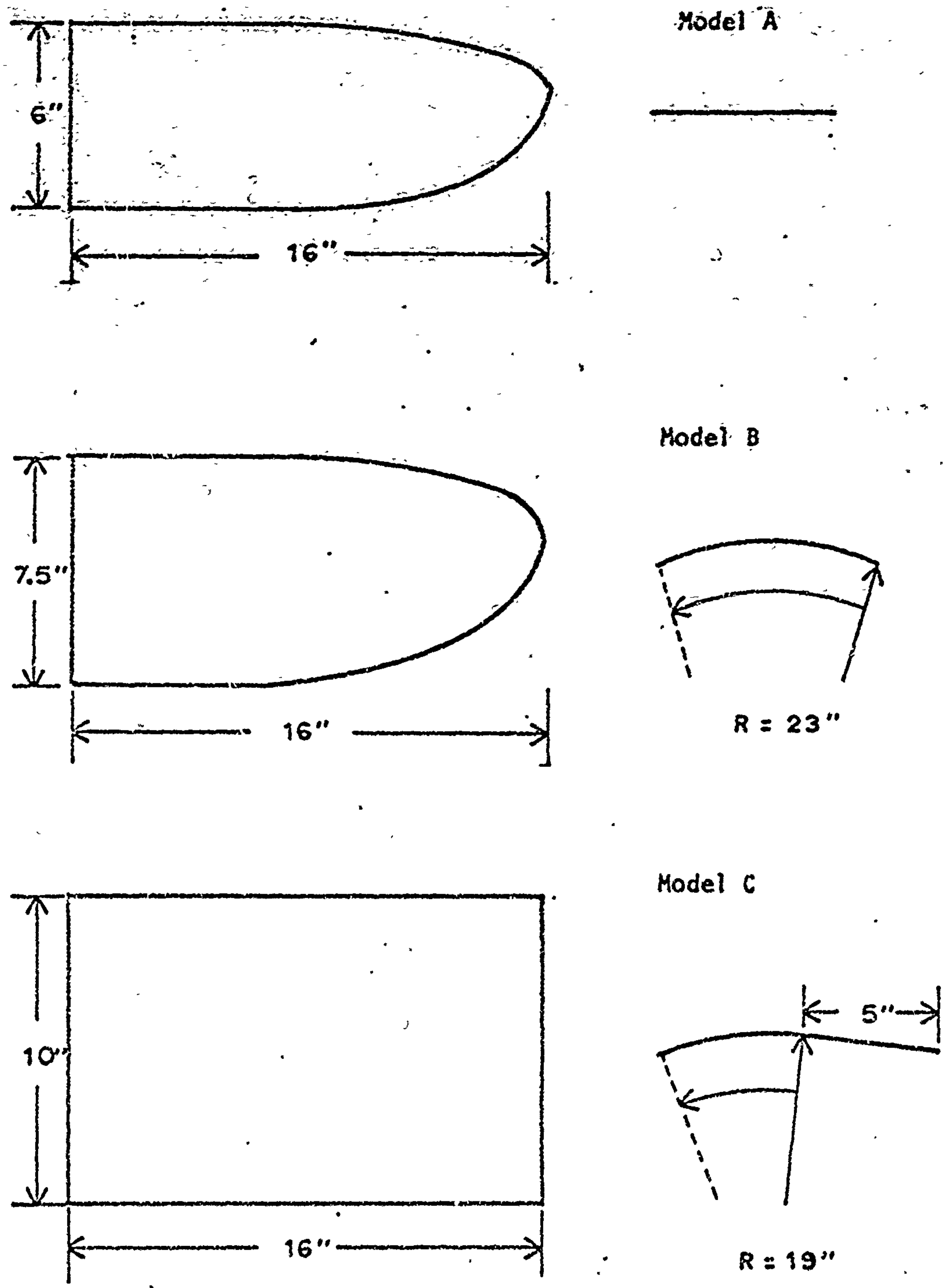

Figure 29. Wing Models

using tweezers. The first design (Figure 30) was constructed by laying off a series of parallel lines oriented at a 25 degree angle to the leading edge. The blades formed by these lines were then given an elliptical taper. The second design represents an attempt to induce a hook shape into the comb. To produce the hook, circular arcs are drawn from positions specified in the dimensions of Figure 31. The two combs of each type illustrate the different shapes that can be obtained by variation of the specified dimensions. Table III gives the dimensions of the combs that were used in the tests. As the table shows, the most successful combs were quite small and difficult to fabricate. To aid in working with such small dimensions, arcs were drawn with a 4 x 0 Rapidograph pen and the parallel lines were applied from dry transfer sheets.

Procedure

Every effort was made to keep the hooked comb and wing models as simple as possible. In the previous sections a number of other devices on the owl wing were identified which could contribute to the mechanism that delays flow separation. Two of the devices were considered for model testing. These were the bastard wing and the slotted wing tip. The bastard wing was modeled with a small winglet cut from shim stock which could be fastened at various positions and angles to the wing surface with modeling clay. The slotted wing tip may also be significant but was not studied here because of the difficulties involved in duplicating its aeroelastic bending and vibration characteristics.

Of the three types of flow visualization methods attempted, only one was successful. A slurry made with titanium dioxide and kerosene

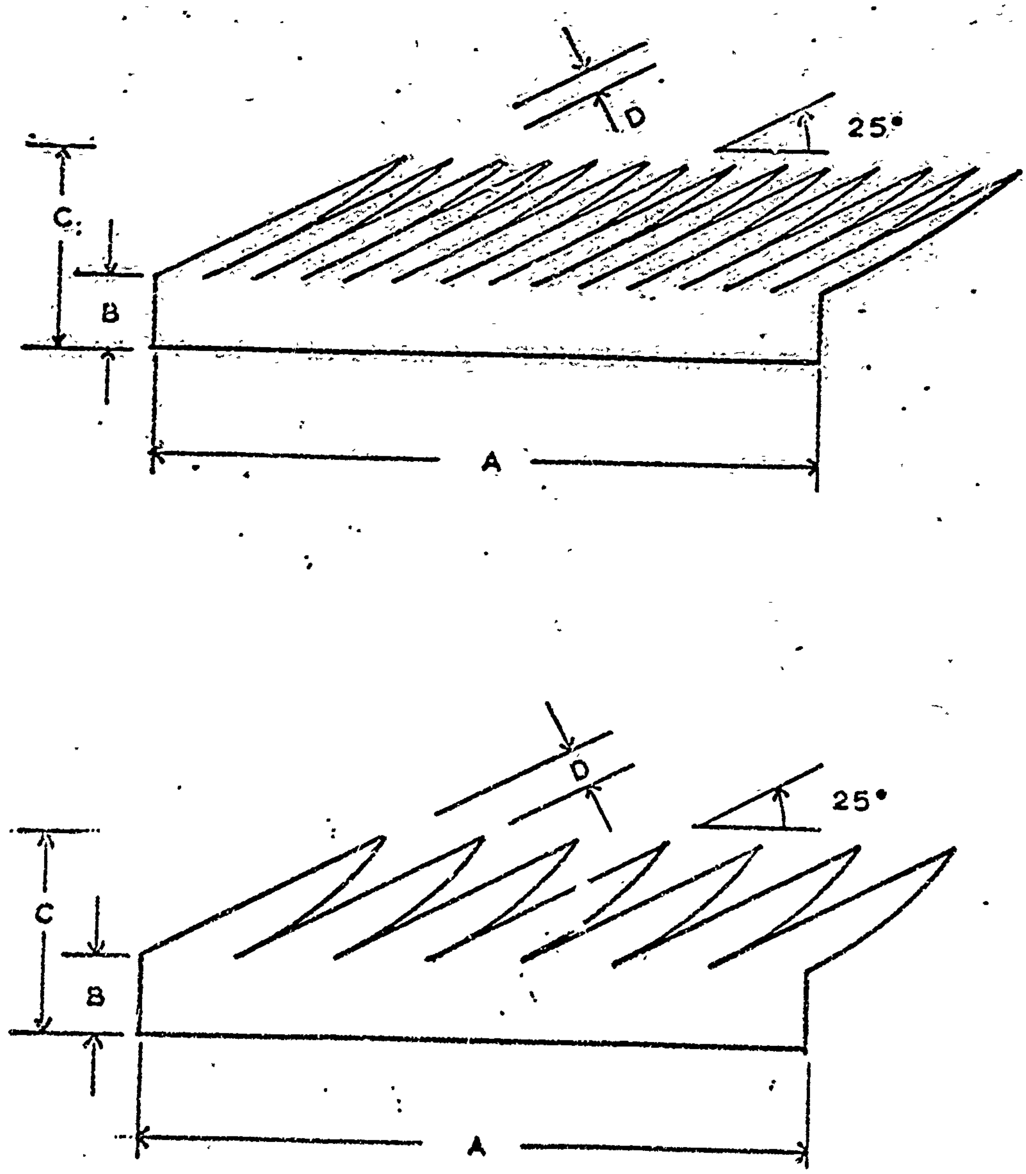

Figure 30. Tapered Comb Models

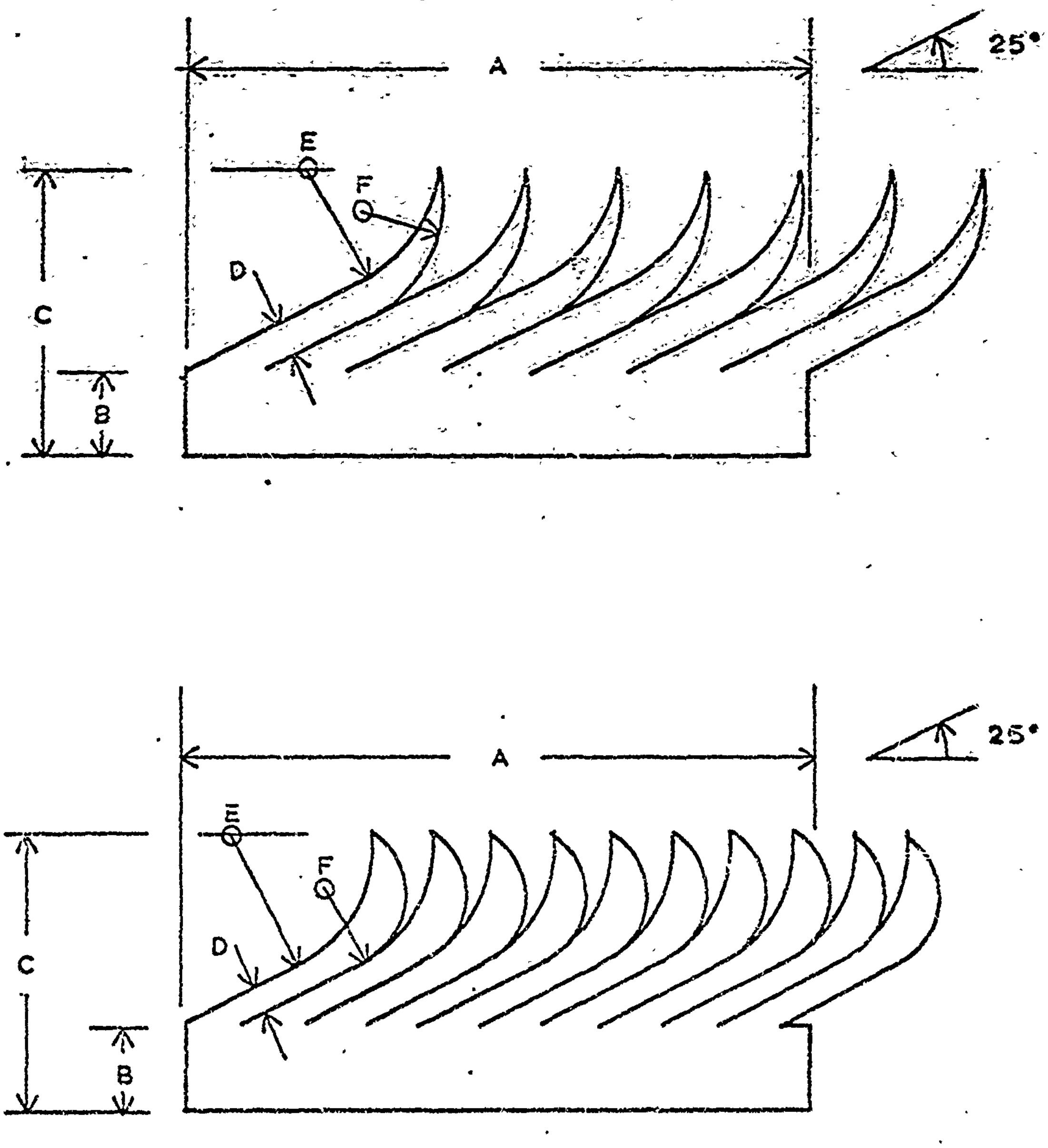

Figure 31. Hooked Comb Models

Table III

Comb Dimensions

	dimensions, in						
Model	A	B	C	D	E	F	High Lift Function
1*	3.0	0.3	0.5	0.08	-	-	No
2	7.5	0.3	0.5	0.05	-	-	"
3	7.5	0.3	0.8	0.05	-	-	"
4	7.5	0.3	0.6	0.03	-	-	"
5	7.5	1.0	1.1	0.05	-	-	"
6	7.5	1.0	1.1	0.03	-	-	Yes
7**	7.5	1.0	1.1	0.03	0.38	0.31	"

*Model 1 has untapered blades.
**Model 7 is constructed using circular arcs.

mixed according to the instructions of reference 15 did not give consistent results because of the low speed range of the wind tunnels. Tufts applied directly to the upper wing surface gave no information on flow behavior above the spanwise vortex region existing behind the comb. The use of smoke was successful in showing the effect of the combs on the flow field when the experimental sequence was:

1. Test each wing model without the comb attached and record stalling angle of attack.
2. Test wing with comb installed.
   a. Check flow through the comb for spanwise turning at high angles of attack.
   b. Check for stationary vortex sheet aft of the comb.
3. Test wing with comb and bastard wing installed and record stalling angle of attack.

VI. Results

The results of the experiment are grouped in three parts. Part 1 represents the preliminary observations of the comb's effect on the flow field at the low tunnel speed of 5 ft/sec. Part 2 shows the high lift function of the comb at increased tunnel speeds of 15 ft/sec, and part 3 relates the comb flow field to that created by spanwise blowing across the wing.

Part 1

The preliminary low speed tests were conducted using the flat plate wing (A). The first five comb models were glued to the upper surface of the wing with the comb blades extending forward over the sharpened leading edge. The low tunnel speed of 5 ft/sec was used to obtain coherent smoke patterns so that detailed streamline behavior could be observed. Smoke flow over the wing prior to fitting the combs (Figure 32) showed that the streamlines proceed directly chordwise. With the combs installed, the flow pattern changes noticeably. At low angles of attack, (Figure 33) the flow through the comb continues chordwise but exhibits considerable stagnation on the wing surface indicating some reduction in flow velocity. At high angles of attack near 30 degrees (Figure 34), the comb turns the flow spanwise toward the wing tip. If the comb extends to the wing tip, the flow through the comb becomes entrained in a stationary vortex core that moves laterally across the wing and rolls up in the trailing tip vortex (Figure 35). Placing the winglet at mid-span (Figure 36) destroyed the vortex. Instead of moving spanwise the flow moved into the region just under the winglet and stagnated. This was likely caused by the winglet inducing attached flow in this area while the rest of the flow on the upper wing surface remained fully separated. Increasing tunnel velocity did not cause attached flow at angles of attack above the plain wing stall. Instead, a classical vortex street was periodically shed from the leading edge (Figure 37). Variations in comb twist and winglet orientation caused no changes in the observed flow patterns. The stationary vortex existed only when the flow was fully separated and the winglet was not installed. To close out the preliminary tests a comb with untapered blades was tried. No stationary vortex was created by this configuration and it was discontinued.

Part 2

None of the comb models were successful in increasing the stalling angle of attack of the flat plate wing (A) or the fully cambered wing (B) using tunnel speeds up to the maximum available of 30 ft/sec. At this point in the experiment, new insight into the theory of the comb operation suggested two changes which proved successful. The first was to more closely model the bionic geometric ratio of comb blade length to wing chord. Wing C in combination with comb 6 or 7 reduced this ratio to 2.5% which approximated more closely the value of 1.8% measured on the owl wing. Second, a sharper leading edge was made by fastening the comb to the bottom surface of the wing. This allowed the .004" shim stock at the base of the comb to become the wing leading edge. The tests of these wing/comb combinations proved successful in delaying flow separation to a marked degree. No difference in performance could be deduced between the two comb models even though they differed greatly in shape and solidity. At a tunnel speed of 15 ft/sec, the stalling angle of attack was delayed from 22 degrees to 30 degrees. Stall could be further delayed up to 35 degrees if the bastard wing was mounted on the wing. The optimum position for the bastard wing was at mid-span with a forward sweep of 45 degrees and raised from the wing surface 30 degrees. Wing performance was very sensitive to changes in bastard wing sweep. Changes in root mounting angle with the wing surface seemed to have much less effect.

A close study of the smoke flow pictures gave considerable insight into the flow mechanism responsible for creating the high lift behavior. Pictures of the wing without the comb installed established the stalling angle of attack to be near 22 degrees (Figure 38). The stall was characteristically abrupt with no sign of transition of oscillation. At angles of attack well above the stall (Figure 39), the flow was fully separated at the leading edge. Installing the comb produced no changes in flow behavior on the wing at angles of attack below 22 degrees. As the angle of attack approached the 22 degrees, however, increasing separation was evident at the wing trailing edge (Figures 40-41). As angle of attack increased above 22 degrees, the flow first became strongly reattached at the trailing edge (Figure 42) and then the vortex region at the leading edge began to grow progressively larger (Figures 43-44). Moving the smoke probe toward the wingtip (Figure 45) showed the vortex region was now smaller in size and of greater intensity. In the regions where the vortex was strong an apparent stagnation point was formed by the smoke flow impinging on the wing surface directly behind the vortex region. As the wing approached the stalling angle of attack (Figure 46), separation was evident at the trailing edge. Stall occurred abruptly (Figure 47) much in the same manner as the plain wing. The nature of the vortex core was examined by injecting smoke into the region just behind the comb (Figure 48). The smoke was entrained in the vortex and outlines its position on the wing. Placing the bastard wing on the model reestablished the vortex flow field at angles of attack up to 34 degrees (Figures 49-51). Again, seperation is evident at the trailing edge just prior to stall.

At the conclusion of the experiment a small owl wing was tested in the smoke tunnel to compare its performance with that of the model. A similar vortex region was observed on the owl wing and the stalling angle of attack agreed within one degree with that of the model.

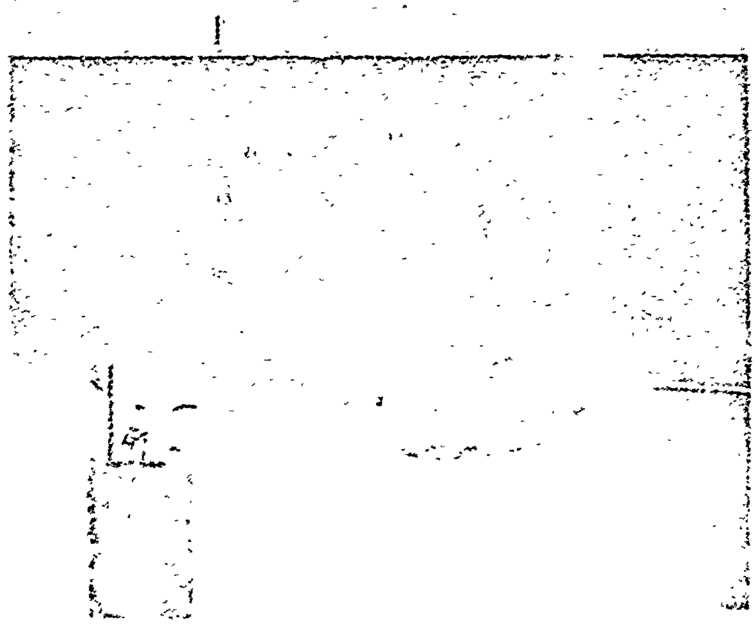

Figure 32. Smoke Flow on Basic Wing Model A
$\alpha = 15°$, V = 5 ft/sec

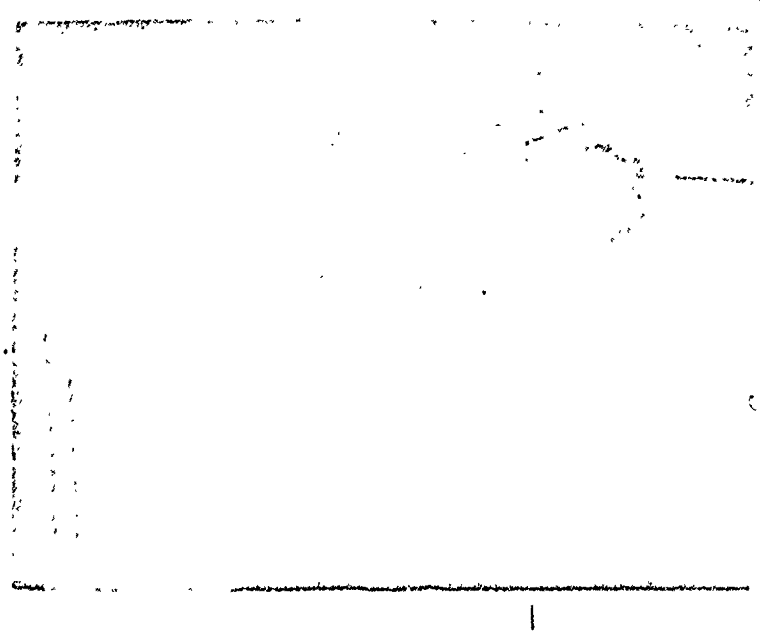

Figure 33. Wing A Fitted with Comb C
$\alpha = 5°$, V = 5 ft/sec

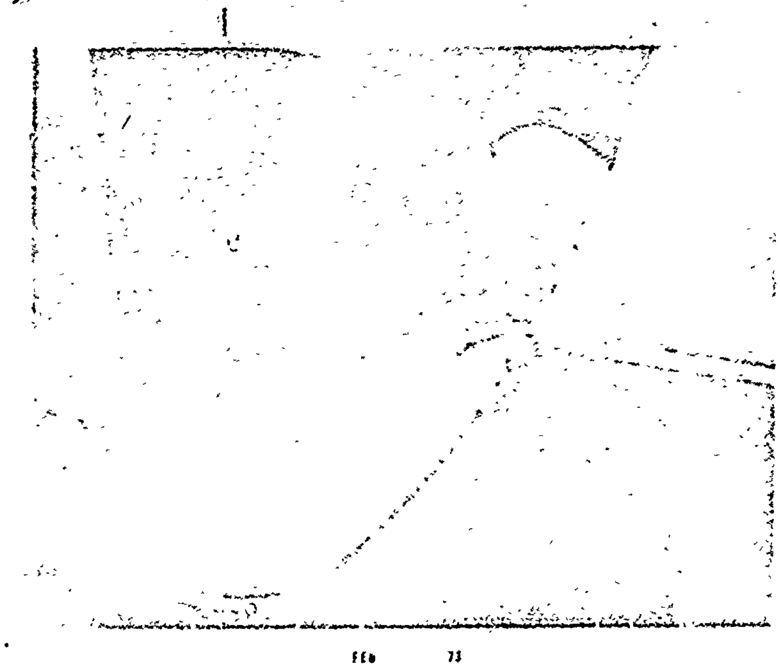

Figure 34. Spanwise Flow Turning
$\alpha = 30°$, V = 5 ft/sec

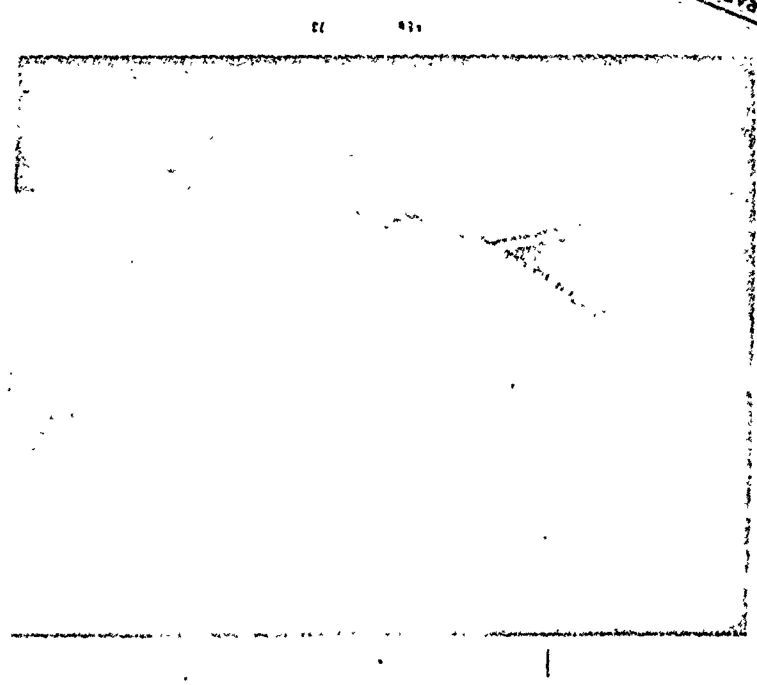

Figure 35. Spanwise Vortex
$\alpha = 30°$, V = 5 ft/sec

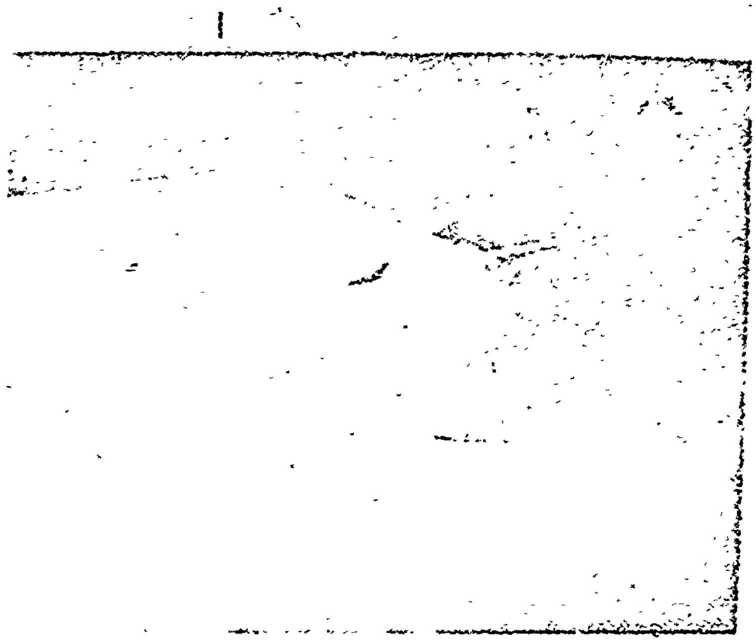

Figure 36. Low Pressure Region Under Bastard Wing
α = 30°, V = 5 ft/sec

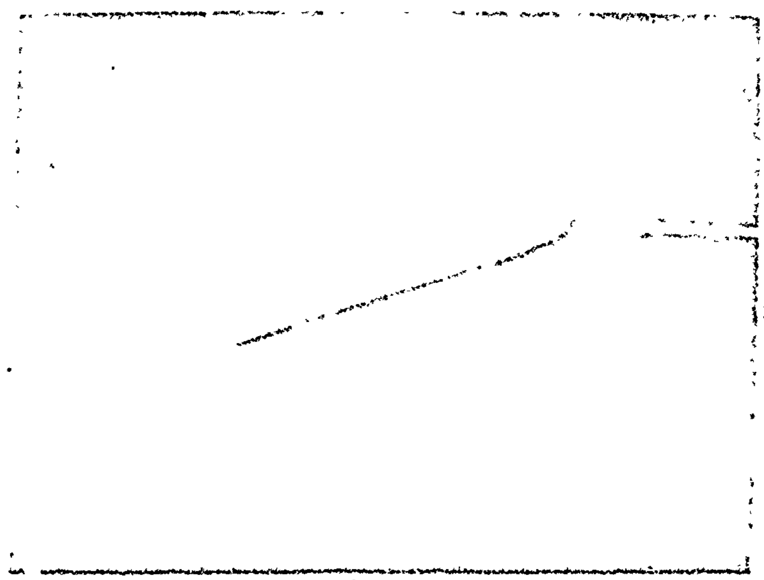

Figure 37. Vortex Street Shed from Wing Leading Edge
α = 20°, V = 15 Ft/sec

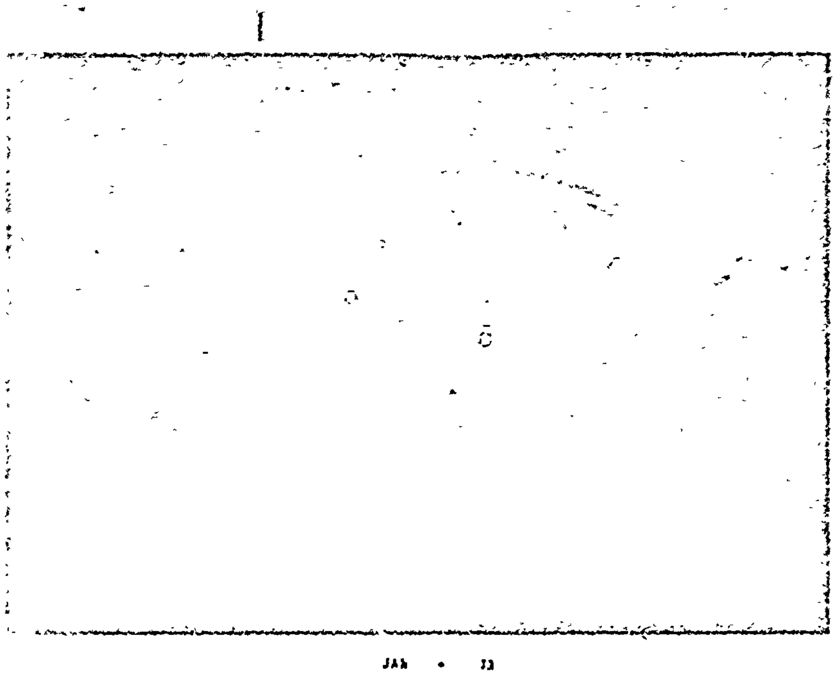

Figure 38. Incipient Stall on Plain Wing Model C
$\alpha = 22°$, V = 15 ft/sec

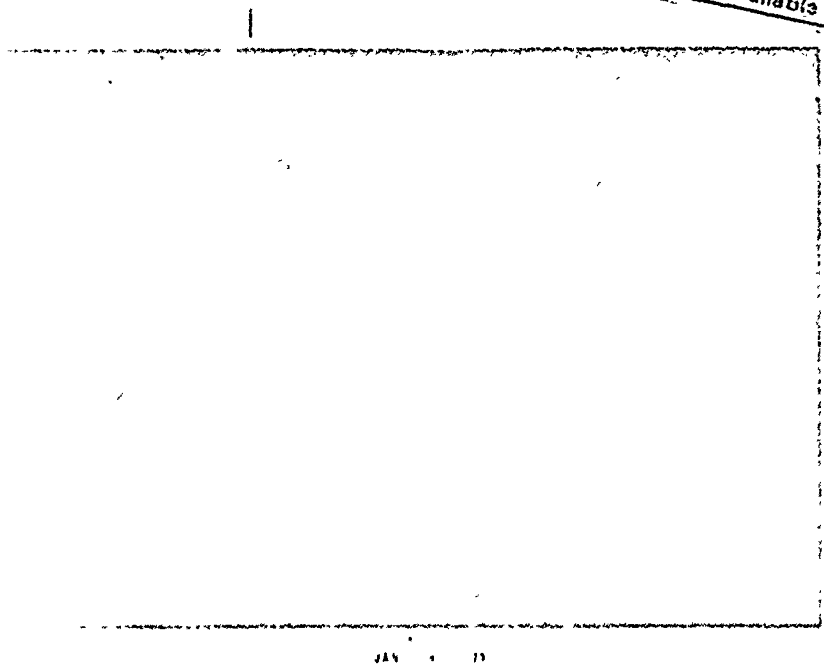

Figure 39. Fully Separated Flow
$\alpha = 27°$, V = 15 ft/sec

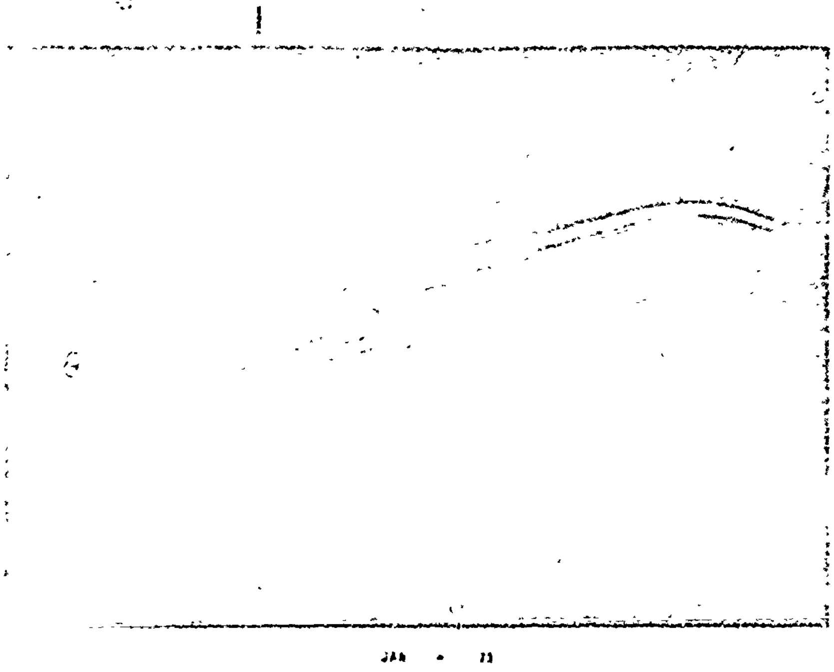

Figure 40. Attached Flow with Comb 6 Installed
$\alpha = 15°$, $V = 15$ ft/sec

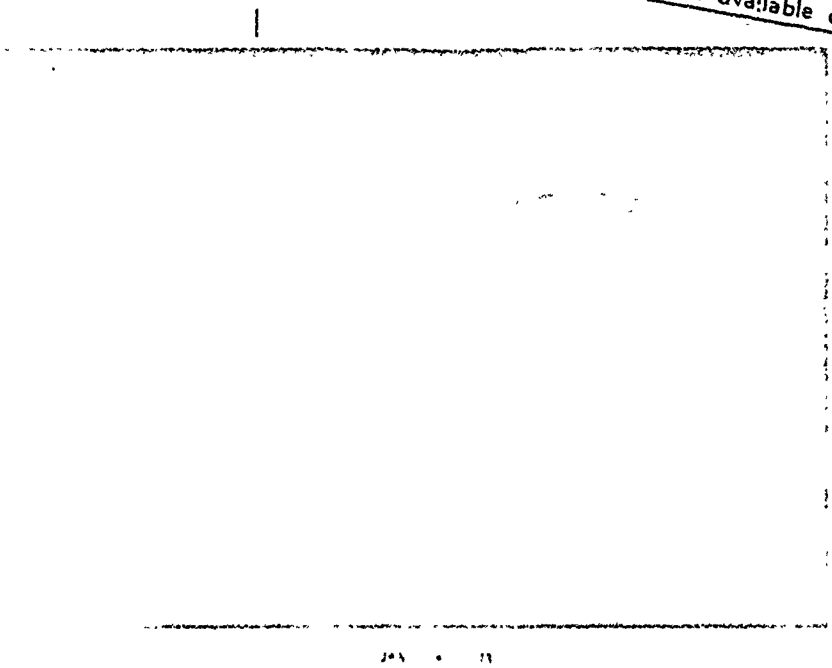

Figure 41. Flow Separation Evident at Trailing Edge
$\alpha = 19°$, $V = 15$ ft/sec

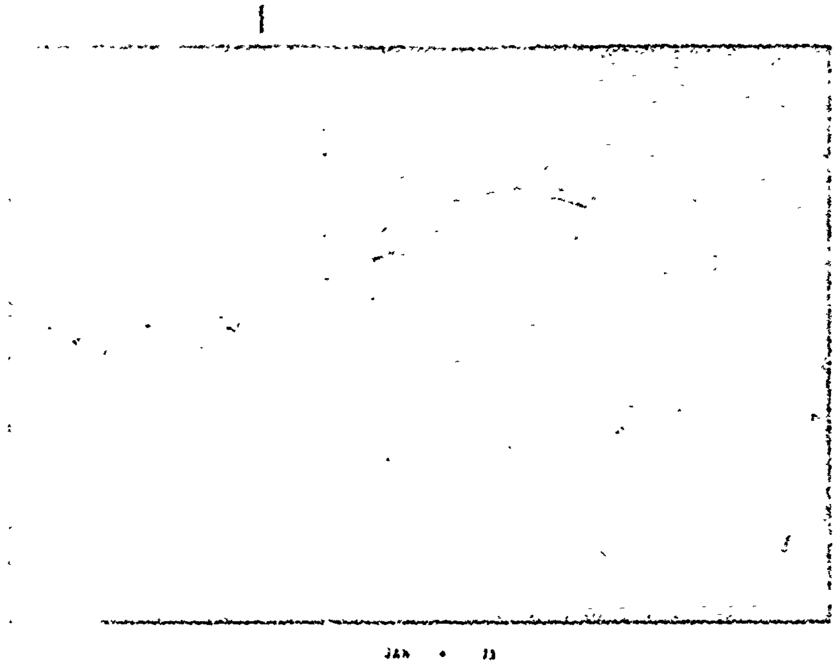

Figure 42. Flow Fully Attached Above Plain Wing Stall
$\alpha = 23°$, $V = 15$ ft/sec

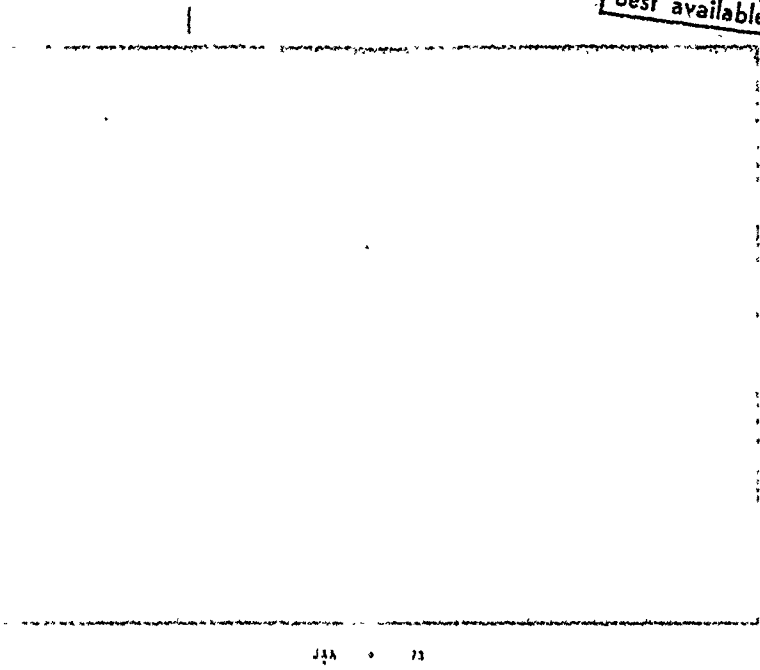

Figure 43. Leading Edge Separation Region Evident
$\alpha = 24°$, $V = 15$ ft/sec

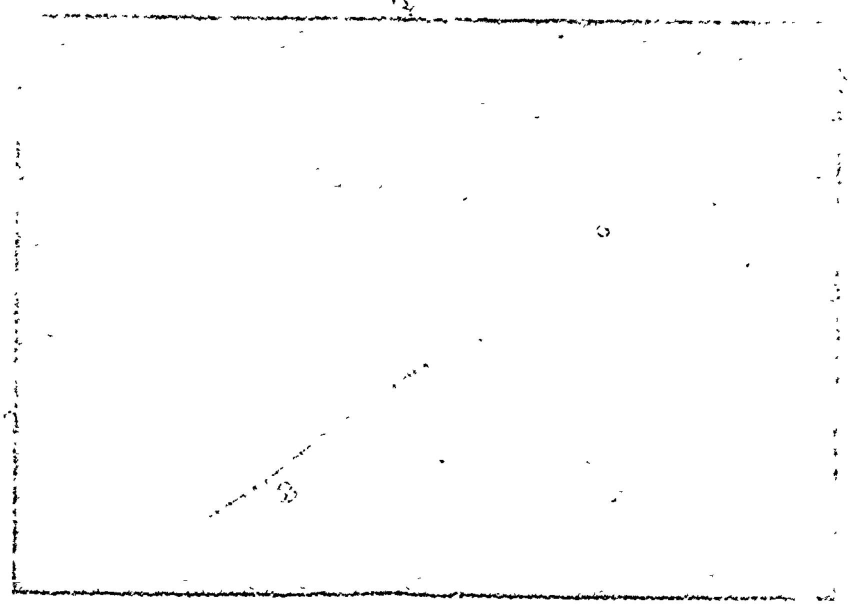

Figure 44. Large Separation Region at 60% Span
$\alpha = 27°$, V = 15 ft/sec

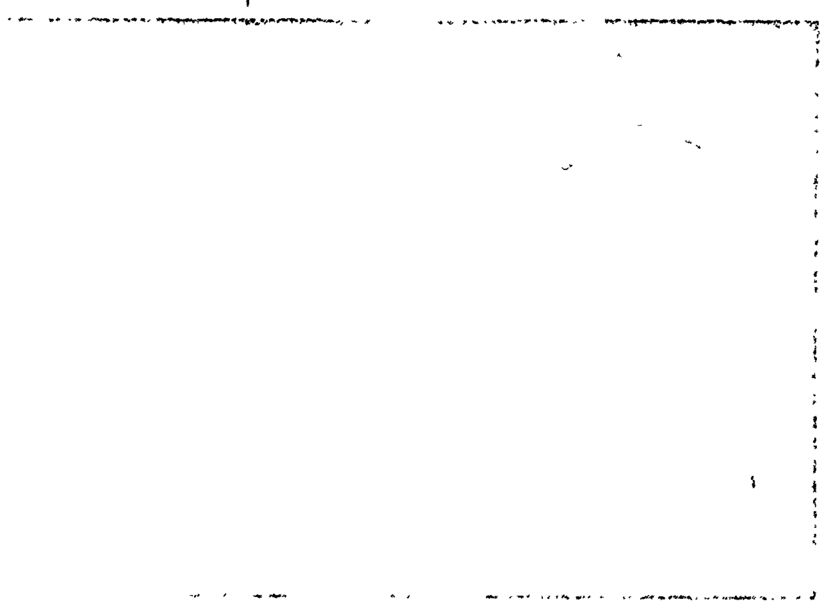

Figure 45. Small Separation Region at 75% Span
$\alpha = 27°$, V = 15 ft/sec

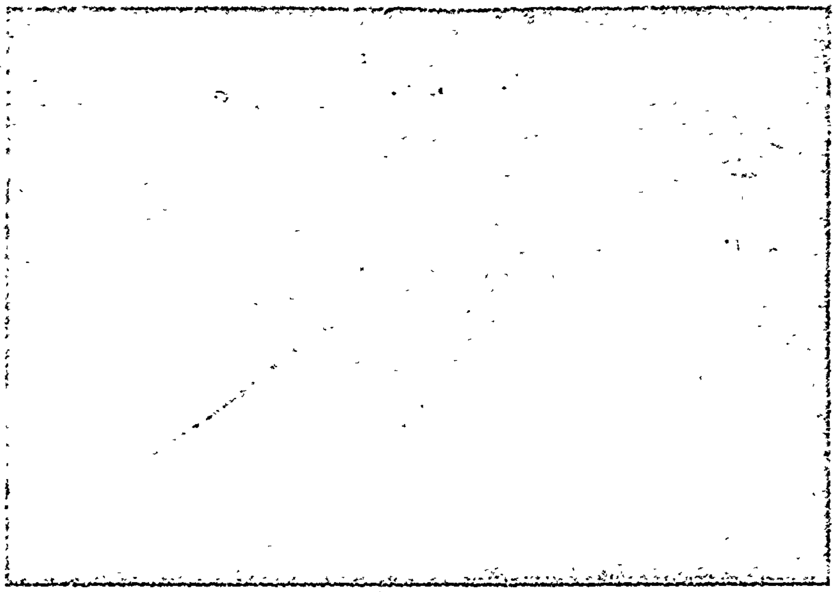

Figure 46. Trailing Edge Separation
$\alpha \approx 29°$, $V \approx 15$ ft/sec

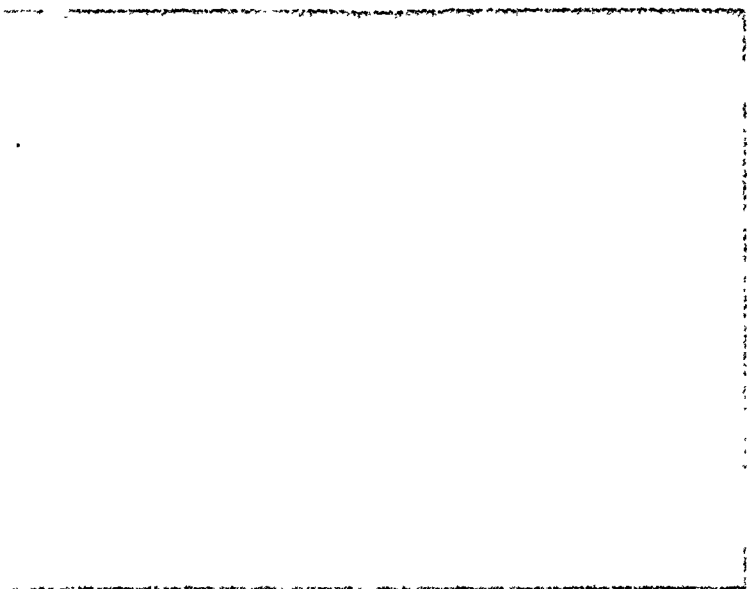

Figure 47. Fully Separated Flow
$\alpha \approx 30°$ $V \approx 15$ ft/sec

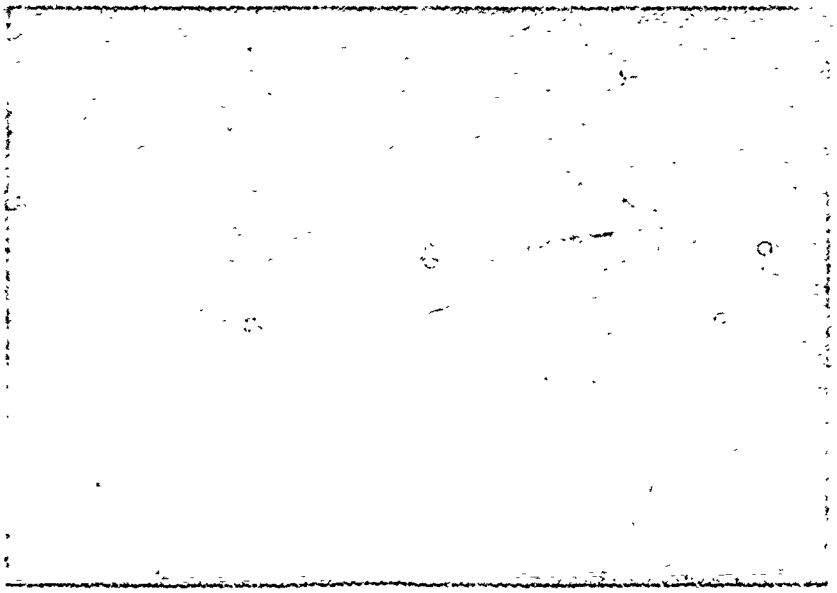

Figure 48. Vortex Core Illuminated
$\alpha = 30°$, V = 15 ft/sec

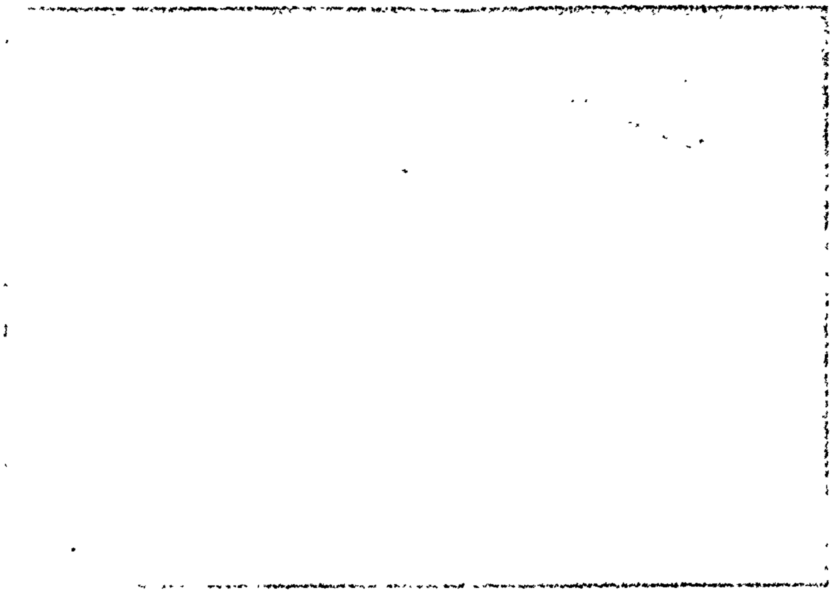

Figure 49. Bastard Wing Installed-Flow Reattaches
$\alpha = 30°$, V = 15 ft/sec

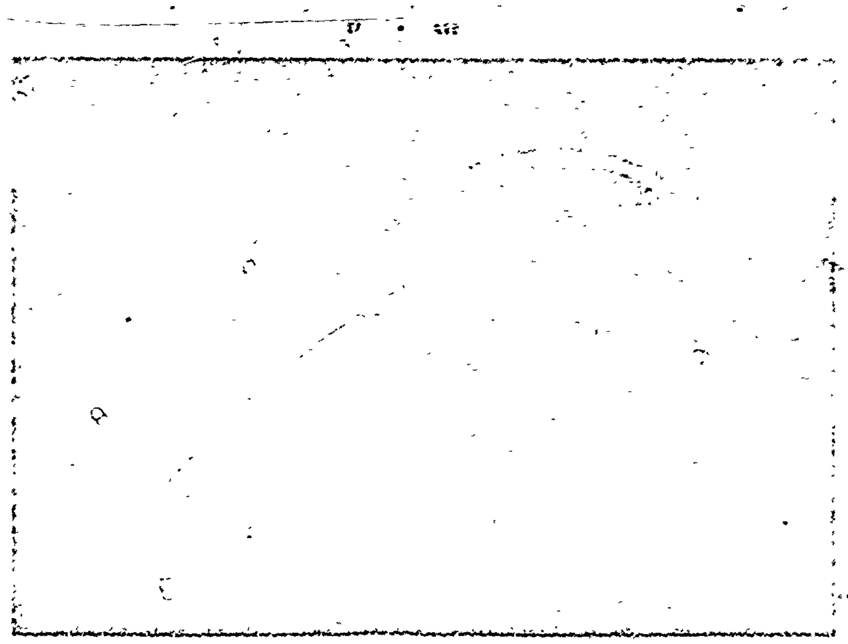

Figure 50. Approaching Stall with Bastard Wing Installed
$\alpha = 34°$, V = 15 ft/sec

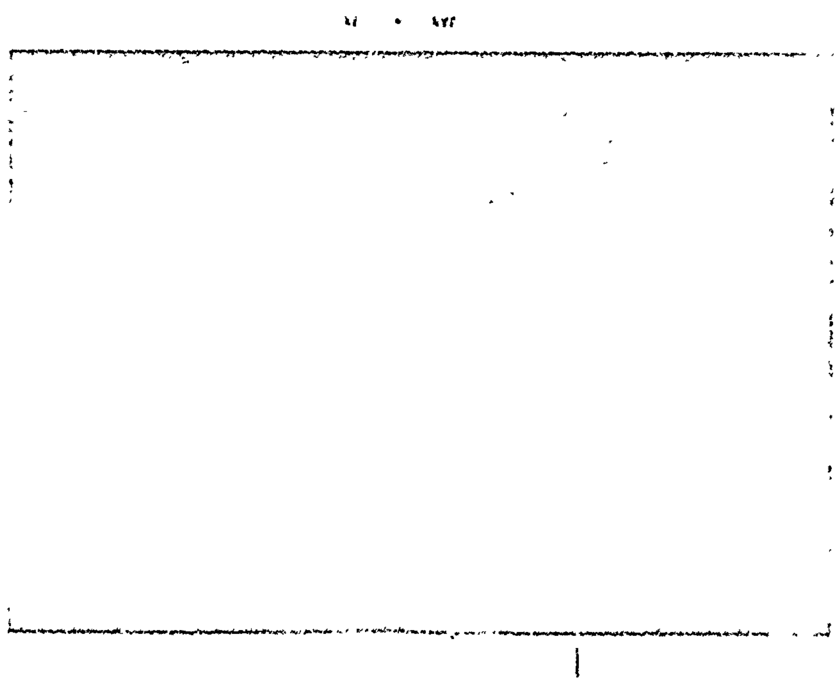

Figure 51. Fully Separated Flow
$\alpha = 40°$, V = 15 ft/sec

Part 3

The flow field seen on a wing equipped with spanwise blowing appears to be the same as that produced by the comb. An air jet was installed at the leading edge of wing C. The jet axis was oriented spanwise and photographs of the flow were made with and without blowing at an angle of attack well above normal wing stall. The test was conducted in the ARL wind tunnel which could provide multiple smoke streams. Figure 52 shows the wing fully stalled. (The air hose obscures the streamlines in the upper left corner of the picture.) In Figure 53 the blowing is on and the vortex region is clearly outlined by the smoke streams. No further tests were run as excellent pictures of spanwise blowing were available for further study in references 16, 17 and 18.

Theory

Vortex Lift. It appears that the comb generates a spanwise leading edge vortex sheet which leads to the high lift characteristics observed in the flow visualization experiments. This vortex sheet is composed of leading-edge-separated vortex filaments that are formed when the flow is unable to negotiate the sharp leading edge of the airfoil and separates. Unswept wings with sharp leading edges shed this vorticity as a periodic vortex street similar to that observed behind bluff bodies. Figure 37 is an excellent example of the vortex street generated by the test wing before the comb was perfected. As the airfoil is swept back in the flow field, the flow changes character. The vortices do not periodically shed from the wing surface but roll up into what is termed a vortex sheet. Figure 54 shows a diagram from Maltby (19) of the vortex sheet produced by a delta wing operating at an angle of attack. In the sketch, the leading-edge-separated vortex distribution is represented by discrete

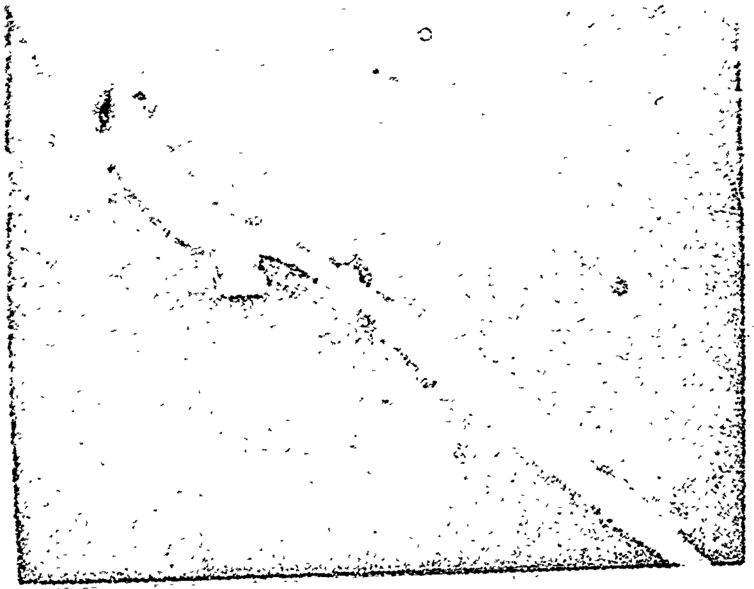

Figure 52. Separated Flow, Blowing Off
$\alpha = 35°$, $V = 25$ ft/sec

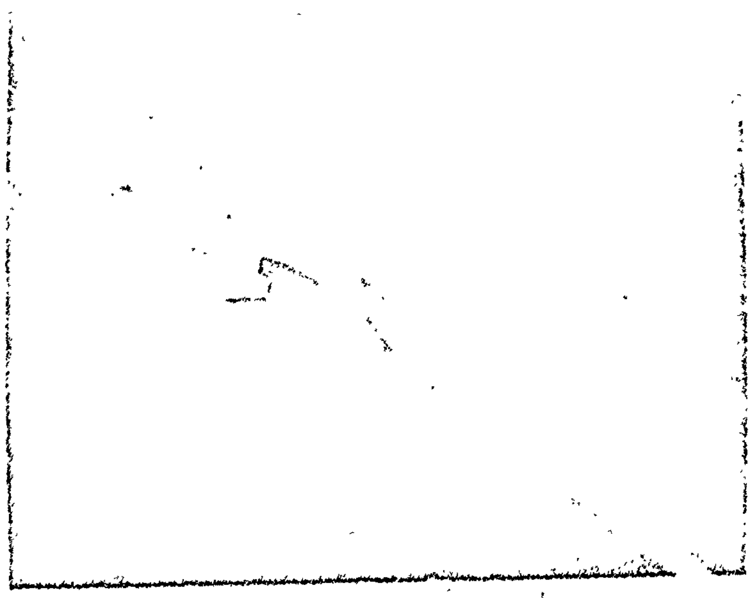

Figure 53. Attached Flow, Blowing On
$\alpha = 35°$, $V = 25$ ft/sec

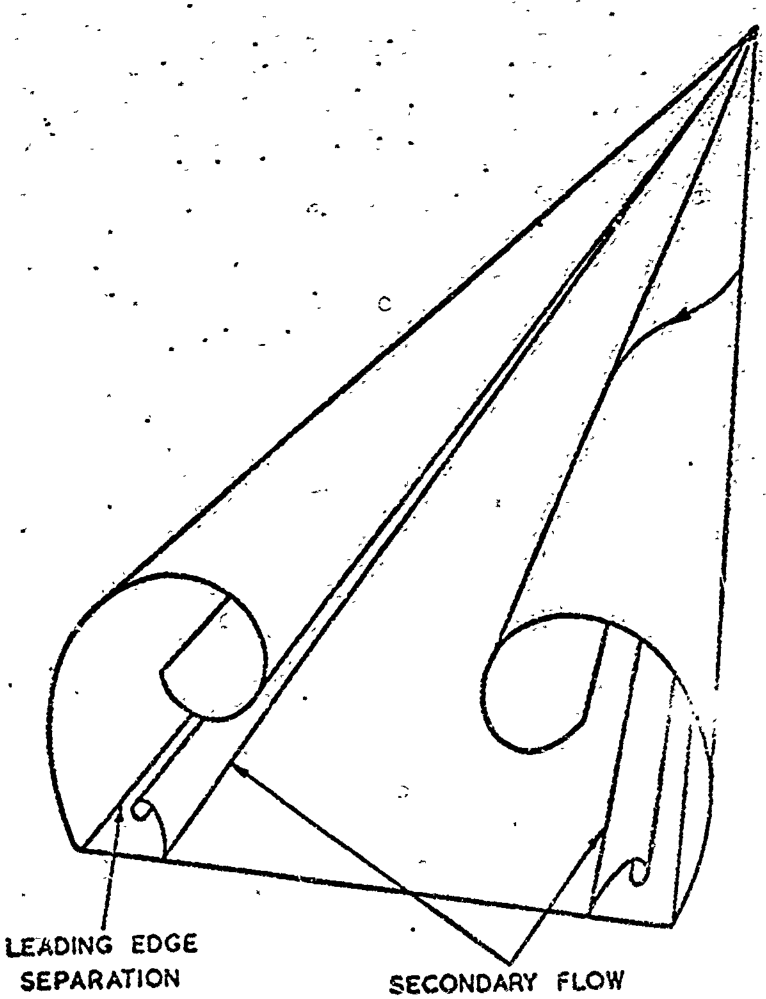

Figure 54. Vortex Sheet on Delta Wing (19)

filaments beginning at the leading edge and rolling up to form a surface. This surface is the so-called vortex sheet and is seen to enclose a core of rotating fluid that grows in size and strength as it flows streamwise along the upper wing surface. The presence of this stationary vortex sheet on the upper wing surface creates a low pressure region of separated flow under the outer flow field. Experiments have shown that the outer flow field flows smoothly over the separated region and reattaches to the wing surface just behind the vortex sheet (20). The lift forces produced by a delta wing are characterized by a non-linear variation with angle of attack. Figure 55 shows typical lift curves for wings with aspect ratios of .5, 1.0, and 2.0. In all three cases the slope of the lift curve increases with angle of attack until $C_{L_{max}}$ is reached. Following Polhamus (21), the lift forces are separated into two components. The first is the conventional linear lift obtained by a solution of the ideal flow about the airfoil. The second component is termed non-linear or vortex lift and is identified by Polhamus as the force resulting from the low pressure field created on the wing surface in the area of the separated flow containing the vortex sheet. Comparison of the increments of lift produced by each component shows two trends. The first is the increase in vortex lift as angle of attack is increased. This can be attributed to the increased vortex shedding which produces lower pressures in the separated region. The second trend is the increase in the ratio of vortex lift to linear lift as the aspect ratio decreases. This is explained by noting that lowering the aspect ratio of the delta wing implies greater sweep which increases the fraction of wing area that is in contact with the vortex sheet. Stall does not usually occur on the delta or swept wing in the

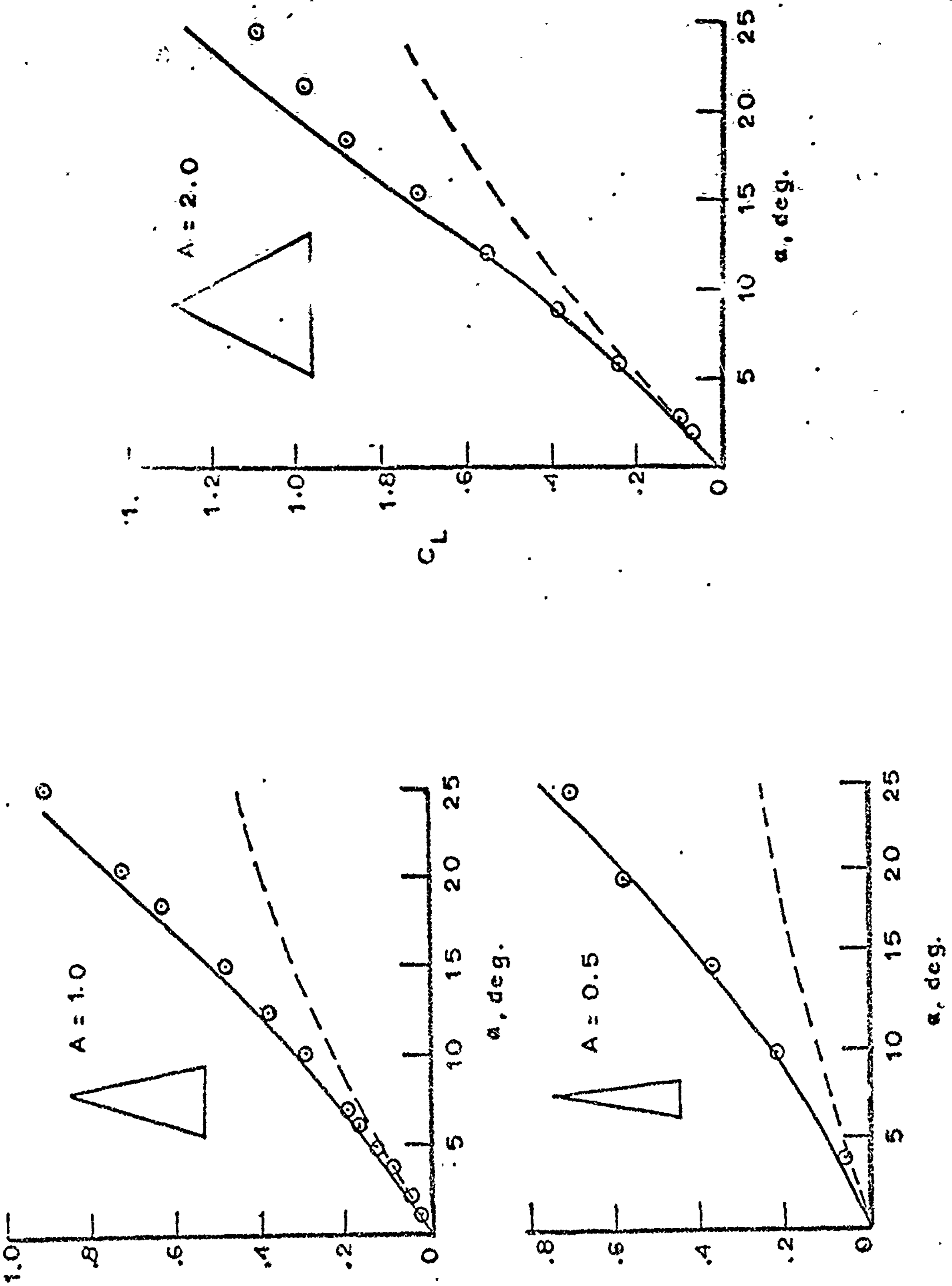

Figure 55. Non-Linear Lift for Several Delta Wings (21)

normal manner. The decrease in C_L after reaching $C_{L_{max}}$ is typically gradual and is accompanied by a large increase in the drag force. The mechanism involved is thought to be a breakdown of the ordered flow in the vortex region that occurs first at the wing trailing edge and travels forward as the angle of attack is increased above $C_{L_{max}}$ (20). The well established flow pattern observed on the delta wing appears to resemble that found on the unswept wing equipped with the leading edge comb. The three elements that allow the vortex sheet to form on the delta wing are seen as: (a) the existence of leading-edge-separated vortices, (b) a spanwise velocity component, and (c) a favorable pressure gradient on the wing surface to prevent vortex breakdown or bursting. In comparison, the experiments with the unswept wing/comb combination show that: (a) leading-edge-separated vortices exist at the sharp leading edge of the wing, (b) spanwise velocities are produced at the wing leading edge by the mechanical turning action of the cascade-like comb, and (c) a favorable spanwise pressure gradient exists at high angles of attack because of the vortex sheet created by the flow around the sharp wing tip region. It should be noted that the existence of the tip vortex alone can contribute sizable non-linear lift increments--especially on rectangular wings of very low aspect ratio. Reference 14 shows this increment to be expressed as,

$$\Delta C_L = C_1 \alpha^2$$

where C_1 represents a coefficient that is based on aspect ratio and planform. A graph of this effect is shown in Figure 56.

<u>Spanwise Blowing</u>. An excellent analogy exists between the flow field produced by the hooked comb and the effect of spanwise blowing

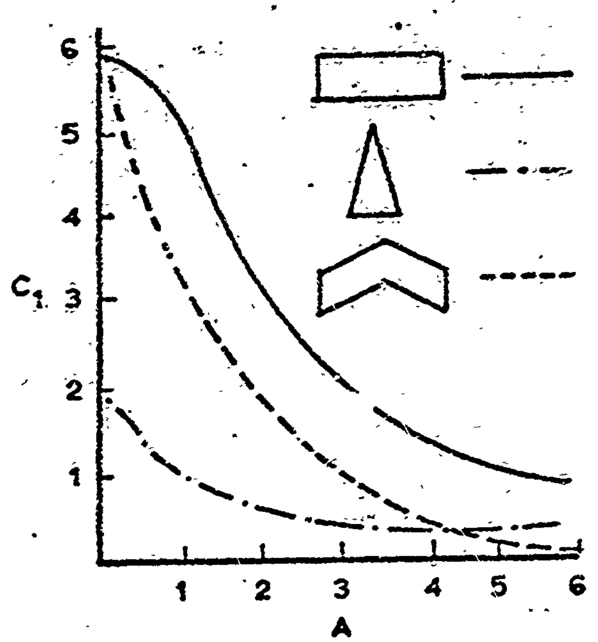

Figure 56. Non-linear Wing-tip Lift for Several Planforms (14)

across an unswept rectangular wing. Dixon (16) and others conducted spanwise blowing tests on a wing similar to those tested in this study and reports flow patterns closely resembling those found in the comb tests. Dixon's model was a flat plate with a sharpened leading edge and had an air jet located at the quarter chord position of the wing root oriented to blow spanwise across the wing. Figure 57 shows a cross section sketch of the streamlines created by the jet at an angle of attack well above the normal flat plate stall. The unique characteristic of this two-dimensional view is the apparent stagnation point that forms on the top of the wing surface just behind the leading edge vortex sheet. When the overall three-dimensional flow field is considered, this point represents a line of division between the flow entrained in the vortex and the exterior field. Figure 58 shows the resulting streamlines on the upper wing surface obtained by Dixon using a slurry for flow visualization. The "herring bone" appearance of the streamlines near the leading edge is like that obtained in similar tests of delta wings (19). While the line of division between the two types of flow is not strictly a stagnation line, there is no streamwise component of velocity and the spanwise velocity is relatively small. This analogy offers an explanation of the unusual line of stagnation reported by Kroeger on the owl wing (6).

Dixon's experiments give some indication of the non-linear lift values achieved by spanwise blowing. Figure 59 shows the lift curves obtained for various degrees of blowing. The blowing coefficient is defined as:

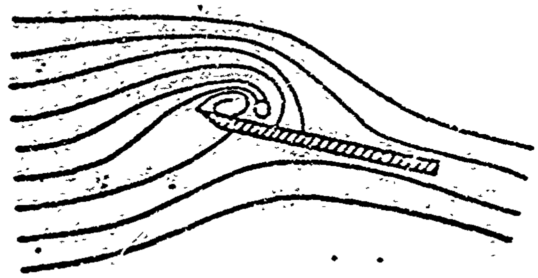

Figure 57. Two-Dimensional Streamlines with Spanwise Blowing (16)

$$C_\mu = \frac{\dot{m}\, V_{jet}}{q\, S}$$

where S represents the wing surface area. To represent the increment of lift actually produced by the spanwise blowing, an additional curve has been superimposed to show the non-linear lift due to tip effects. This was computed using the method of reference 14.

Bastard Wing. The comb experiment also considered the effects of the bastard wing on the flow field as it was previously assumed to be working in conjunction with the comb. Including a small winglet at mid-span did result in higher values of stalling angle of attack in the smoke visualization experiments. This was unusual performance if the winglet is considered to be functioning only as a conventional leading edge slat. In addition to the slat effect, however, a vortex field is produced by the bastard wing. This is shown in Figure 60. The forward sweep of the winglet produces a leading edge vortex sheet whose sense of rotation is counter-clockwise looking upstream. The conventional trailing edge vortex system is seen to have the opposite sense. Considering its small relative size, it is possible that the bastard wing operates in conjunction with its vortex field

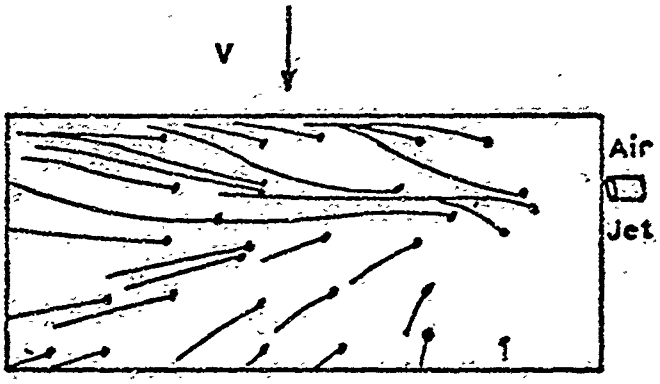

Figure 58. Three-Dimensional Surface Flow Marked with Slurry (16)

to produce a spanwise fence to oppose the propagation of separated flow from the root area of the main wing. At any rate, the unusual counter-rotating flow field described by Kroeger (6) is likely due to the presence of the bastard wing.

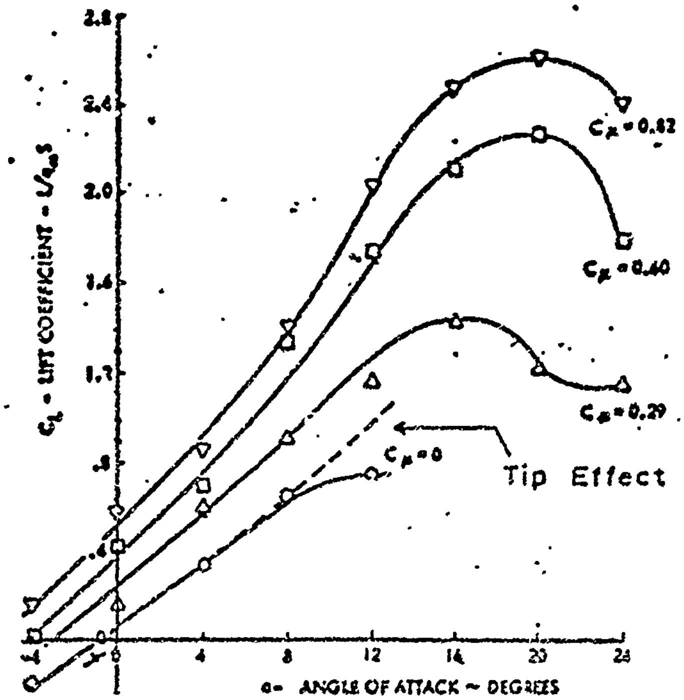

Figure 59. Lift Curves Obtained for Various Degrees of Blowing (16)

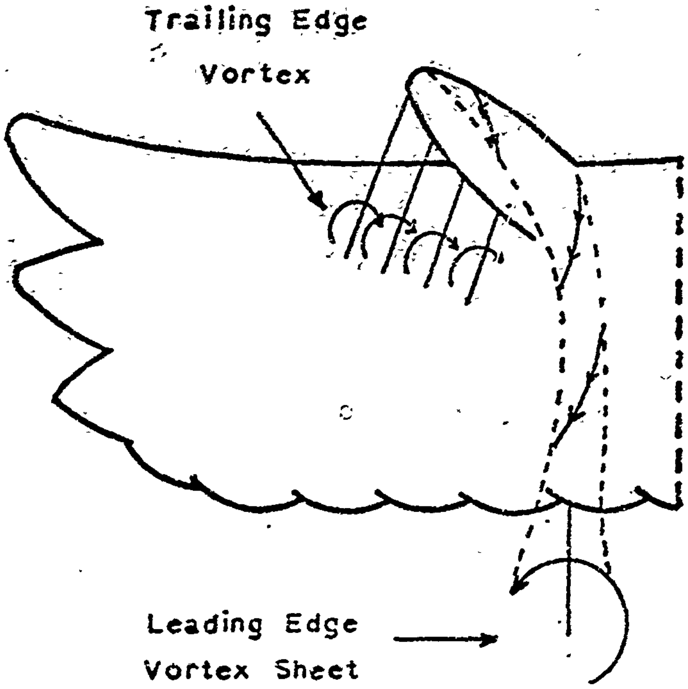

Figure 60. Vortex Sheets Generated by the Bastard Wing

VII. Conclusions and Recommendations

The results of the study of the owl wing and the experiments with the hooked comb suggest the following conclusions:

1. The hooked comb present on the owl wing works in conjunction with a sharp leading edge to produce non-linear lift on the outer half of the wing.
2. A working model of the comb system can be made from sheet metal. The critical parameters in the comb construction are thought to be:
   a. A comb blade length to wing chord ratio near 1.8%.
   b. Slanting the comb blades at a 25 degree angle relative to the wing leading edge. This slant is toward the wingtip.
   c. The individual blades must be tapered.
3. The comb turns the flow only at high angles of attack. At flight angles of attack, the comb presents an extremely small drag profile.
4. The small relative size of the comb (1.8%) makes it attractive for use as an aircraft high lift device. It is specifically suited for aircraft possessing unswept wings with sharp leading edges.
5. The flow field created by spanwise blowing is very similar to the flow field created by the hooked comb.
6. The bastard wing, extended on the upper surface of the owl wing during gliding flight, may act as a fence to

delay outward propagation of flow separation from the thick and highly cambered wing root sections.

7. Potential applications of the comb's principle of operation can be envisioned in the fields of fluidics and combustion chamber design. Several fluidic devices already developed use separated flow to alter the performance of a nozzle. In turbojet engines, shorter combustion chamber design hinges in part on improved means of combining the air/fuel mixture. The hooked comb deserves consideration in both these applications as it appears to be the first unpowered device reported in the literature that creates a stationary vortex sheet oriented at right angles to the direction of flow.

The following recommendations are made:

1. Further wind tunnel tests should be conducted using a hooked comb model to measure aerodynamic forces and refine the concept of non-linear lift.
2. Larger models should be considered for any new wind tunnel tests as the small relative size of the comb makes accurate fabrication difficult.

Bibliography

1. Graham, R.R. "The Silent Flight of Owls". Journal of the Royal Aeronautical Society, 38: 837-843 (1934).

2. Raspet, August. "Biophysics of Bird Flight". Science, 132: 191-199 (July 1960).

3. Blick, E.F. "Bird Aerodynamics". Soaring, 36: 26-31 (June 1972).

4. Soderman, Paul T. Aerodynamic Effects of Leading-Edge Serrations on a Two Dimensional Airfoil. NASA Technical Memorandum X-2643. Washington: National Aeronautics and Space Administration, September 1972.

5. Hertel, Heinrich. Structure-Form-Movement. New York: Reinhold Publishing Corp., 1966.

6. Kroeger, R.A., et al. Low Speed Aerodynamics for Ultra Quiet Flight. AFFDL-TR-71-75. Wright-Patterson AFB, Ohio: AF Flight Dynamics Laboratory, March 1972.

7. Shestakova, G.S. The Problem of the Penetrability of Bird's Wings. Royal Aircraft Establishment Library Translation 1143: Farnborough: Ministry of Aviation, December 1965. AD 804465.

8. Vinogradov, I.N. The Aerodynamics of Soaring Bird Flight. Royal Air-Royal Aircraft Establishment Library Translation 846. Farnborough: Ministry of Aviation, January 1960. AD 234631.

9. Gerardin, L. Bionics. New York: McGraw-Hill Book Company, 1968.

10. Kramer, M.O. "Boundary-Layer Stabilization by Distributed Damping." Journal of Aeronautical Science, 24: 459-460 (June 1957).

11. Spark, John. Owls: Their Natural and Unnatural History. New York: Taplinger Publishing Company, 1970.

12. Taylor, John W., Editor. Jane's All the World's Aircraft. New York: McGraw-Hill Publishing Company, 1970.

13. Jacobs, E.N. The Characteristics of 78 Related Airfoil Sections From Tests in the Variable Density Wind Tunnel. NACA Report No. 460. Washington: National Advisory Committee for Aeronautics, 1935.

14. Nicolai, Leland M. Design of Airlift Vehicles. Colorado Springs: United States Air Force Academy, July 1972.

15. Maltby, R.L. and Keating, R.F.A. Flow Visualization in Low-Speed Wind Tunnels. RAE Technical Report Aero 2715. London: Royal Aircraft Establishment, 1960. AD 245348.

16. Dixon, C.J. Lift Augmentation by Lateral Blowing Over a Lifting Surface. AIAA Paper No. 69-193. Washington: American Institute of Aeronautics and Astronautics, February 1969.

17. Werle, H. and Gallon, M. Controle dEcoulements par Jet Transversal. O.N.E.R.A. T.P. 1070. Chatillon: Office National dEtudes it de Recherches Aerospatiales, 1972.

18. Carafoli, E. and Camarasescu, N. New Researches on Small Span-Chord Ratio Wings with Lateral Jets. FTD Translation HC-23-319-71. Wright-Patterson AFB, Ohio: Foreign Technology Division, USAF, 1971.

19. Maltby, R.L. "The Development of the Slender Delta Concept". Aircraft Engineering, XL: 12-17 (March 1968).

20. Chang, Paul K. Separation of Flow. New York: Pergamon Press, 1970.

21. Polhamus, E.C. A Concept of the Vortex Lift of Sharp-Edge Delta Wings Based on a Leading Edge Suction Analogy. NASA TN D-3767. Washington: National Aeronautics and Space Administration, December 1966.

Vita

George William Anderson was born on 26 November 1941 in Greenville, Pennsylvania. He graduated from Pymatuning Joint High School in Jamestown, Pennsylvania in 1959 and enlisted in the Air Force the same year. After completing basic training, he was assigned to the United States Naval Academy Preparatory School at Bainbridge Naval Training Center, Maryland. In 1960, he entered the United States Air Force Academy and graduated in 1964 with a Bachelor of Science degree and a commission as a Second Lieutenant in the Air Force. After graduating from pilot training at Reese AFB, Texas in 1965, he was assigned to the 29th Military Airlift Squadron at McGuire AFB, N.J. as a C-130E pilot. In 1967-68, he served with the 362nd Tactical Electronic Warfare Squadron at Pleiku, RVN as an RC-47 pilot. From 1968 until entering AFIT in 1971, he served with the 30th Military Airlift Squadron at McGuire AFB, N.J. as a C-141A instructor pilot and flight examiner.

Permament address: Liberty Street
Jamestown, Pennsylvania, 16146

This thesis was typed by Katherine Randall